Treball de Fi de Màster

Màster Universitari en Enginyeria Industrial

Volum II/II

Verificació analítica i numèrica de la patent EP 2305911 aplicada a una xapa nervada comercial per lloses mixtes.

ANNEX

Autor: Carla Ripoll Martínez
Director: Frederic Marimon Carvajal
Miquel Ferrer Ballester
Convocatòria: Abril 2019

ETSEIB

Escola Tècnica Superior
d'Enginyeria Industrial de Barcelona

UPC

Sumari

A. PROPIETATS ELÀSTIQUES EFICACES DE LA SECCIÓ

A continuació es detallen els càlculs de la secció elàstica eficaç per les diferents xapes, segons el procediment detallat a l'apartat 5.3. de la memòria. Aquestes propietats, al dependre de les tensions, s'ha de diferenciar entre aplicació de moment flector positiu i moment flector negatiu.

A.1. Perfil KORONA 60

Les dimensions geomètriques de la secció són les següents, mostrades en la Fig. A.1 i Taula A.1.

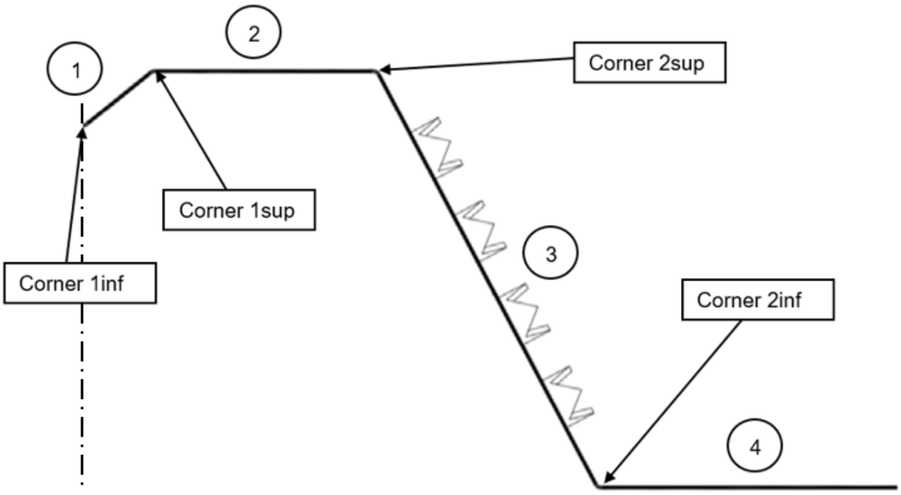

Fig. A.1. Parts que composen la secció del element KORONA 60.

Element	b_{pi}(mm)
1	12,67
2	31,65
3	66,31
4	28,71

Taula A.1. Dimensions geomètriques principals.

En les zones de corner hi han les següents dimensions:

r = 3 mm

$\theta_1 = 38{,}66°$

$\theta_2 = 62°$

A.1.1. Moment positiu

A.1.1.1. Ala superior

Mitjançant el procediment detallat en l'Eurocodi 3 es pot trobar l'esveltesa relativa pels diferents gruixos.

$$\overline{\lambda_p}(0{,}75) = \sqrt{\frac{f_{yb}}{\sigma_{cr}}} = \frac{\frac{\bar{b}}{t}}{\left(28{,}4 \cdot \varepsilon \cdot k_\sigma{}^{\frac{1}{2}}\right)} = 0{,}99$$

$$\overline{\lambda_p}(1{,}00) = \sqrt{\frac{f_{yb}}{\sigma_{cr}}} = \frac{\frac{\bar{b}}{t}}{\left(28{,}4 \cdot \varepsilon \cdot k_\sigma{}^{\frac{1}{2}}\right)} = 0{,}74$$

$$\overline{\lambda_p}(1{,}20) = \sqrt{\frac{f_{yb}}{\sigma_{cr}}} = \frac{\frac{\bar{b}}{t}}{\left(28{,}4 \cdot \varepsilon \cdot k_\sigma{}^{\frac{1}{2}}\right)} = 0{,}61$$

$$\varepsilon = \sqrt{\frac{235}{f_{yb}}} = 0{,}79$$

El factor de vinclament utilitzat és $k_\sigma = 4$ i $\bar{b} = b_{p2}$.

Ja es pot calcular el factor reductor ρ que varia segons el material utilitzat. En el cas que ens pertoca, per l'acer, s'utilitzarà la següent formula:

$$\rho\ (0{,}75) = \frac{1 - 0{,}55 \cdot \frac{(3+\psi)}{\overline{\lambda_p}}}{\overline{\lambda_p}} = 0{,}78$$

$$\rho\ (1{,}00) = \frac{1 - 0{,}55 \cdot \frac{(3+\psi)}{\overline{\lambda_p}}}{\overline{\lambda_p}} = 0{,}95$$

$$\rho\ (1{,}20) = \frac{1 - 0{,}55 \cdot \frac{(3+\psi)}{\overline{\lambda_p}}}{\overline{\lambda_p}} = 1{,}00$$

El rati de tensions (σ_2/σ_1) és $\psi=1$.

Aquest factor en indica si cal considerar que la regió $\bar{b}$ en tota la seva longitud és o no efectiva. Per tant la longitud eficaç de la zona plana de l'ala és:

$$b_{eff}(0{,}75) = \rho \cdot \bar{b} = 24{,}80\ mm$$

$$b_{eff}(1{,}00) = \rho \cdot \bar{b} = 30{,}20\ mm$$

$$b_{eff}(1{,}20) = \rho \cdot \bar{b} = 31{,}63\ mm$$

La longitud utilitzada és $\bar{b} = b_{p2}$

S'obté l'àrea eficaç de la part dels rigiditzadors de l'ala superior. S'utilitza el procediment indicat en la normativa EN 1993-1-3:2006 [2]. Primer es calcula una secció eficaç (Taula A.2) utilitzant les especificacions de la Fig. A.2.

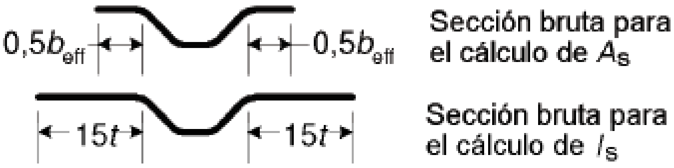

Fig. A.2. Figura 5.11 de EN 1993-1-3:2006 [2].

Element	**t = 0,75**		**t = 1,00**		**t = 1,20**	
	L_i (mm)	**A_i (mm^2)**	**L_i (mm)**	**A_i (mm^2)**	**L_i (mm)**	**A_i (mm^2)**
Part plana (Fig. A.2)	11,29	8,01	13,93	13,37	14,63	16,97
Corner 1sup	2,26	1,61	2,35	2,25	2,42	2,80
1	10,45	7,42	10,36	9,95	10,29	11,94
Corner 1inf	2,26	1,61	2,35	2,25	2,42	2,80
Corner 1inf	2,26	1,61	2,35	2,25	2,42	2,80
1	10,45	7,42	10,36	9,95	10,29	11,94
Corner 1sup	2,26	1,61	2,35	2,25	2,42	2,80
Part plana (Fig. A.2)	11,29	8,01	13,93	13,37	14,63	16,97
TOTAL		**37,30**		**55,66**		**69,03**

Taula A.2. Primer càlcul de la secció eficaç de l'ala superior.

També s'obté una primera inèrcia eficaç (Taula A.3) segons la Fig. A.2.

Element	**L_i (mm)**	**A_i (mm^2)**	**Z (mm)**	**S_i (mm^3)**	**z_0 (mm)**	**I_i (mm^4)**
Part plana (Fig. A.2)	9,54	6,77	0,00	0,00	2,48	41,90
Corner 1sup	2,30	1,61	0,19	0,30	2,29	8,43
1	10,50	7,42	4,00	29,69	-1,52	43,73
Corner 1inf	2,30	1,61	8,19	13,16	-5,71	52,41
Corner 1inf	2,30	1,61	8,19	13,16	-5,71	52,41
1	10,5	7,42	4,00	29,69	-1,52	43,73
Corner 1sup	2,30	1,61	0,19	0,30	2,29	8,43
Part plana (Fig. A.2)	9,54	6,77	0,00	0,00	2,48	41,90
TOTAL		34,82		86,30	2,48	**292,94**

Taula A.3. Primer càlcul del moment inèrcia eficaç de l'ala superior. t = 0,75.

Element	**L_i (mm)**	**A_i (mm^2)**	**Z (mm)**	**S_i (mm^3)**	**z_0 (mm)**	**I_i (mm^4)**
Part plana (Fig. A.2)	13,25	12,72	0,00	0,00	2,16	60,35
Corner 1sup	2,30	2,25	0,20	0,44	1,96	8,70
1	10,40	9,95	4,00	39,80	-1,84	68,89
Corner 1inf	2,30	2,25	8,20	18,48	-6,04	82,11
Corner 1inf	2,30	2,25	8,20	18,48	-6,04	82,11
1	10,40	9,95	4,00	39,80	-1,84	68,89
Corner 1sup	2,30	2,25	0,20	0,44	1,96	8,70
Part plana (Fig. A.2)	13,25	12,72	0,00	0,00	2,16	60,35
TOTAL		54,35		117,44	2,16	**440,11**

Taula A.4. Primer càlcul del moment inèrcia eficaç de l'ala superior. t = 1,00.

Element	**L_i (mm)**	**A_i (mm^2)**	**Z (mm)**	**S_i (mm^3)**	**z_0 (mm)**	**I_i (mm^4)**
Part plana (Fig. A.2)	16,21	18,81	0,00	0,00	1,96	74,49
Corner 1sup	2,40	2,80	0,20	0,57	1,76	8,68
1	10,30	11,94	4,00	47,77	-2,04	91,59
Corner 1inf	2,40	2,80	8,20	22,98	-6,24	109,11
Corner 1inf	2,40	2,80	8,20	22,98	-6,24	109,11
1	10,30	11,94	4,00	47,77	-2,04	91,59
Corner 1sup	2,40	2,80	0,20	0,57	1,76	8,68
Part plana (Fig. A.2)	16,21	18,81	0,00	0,00	1,96	74,49
TOTAL		72,71		142,63	1,96	**567,74**

Taula A.5. Primer càlcul del moment inèrcia eficaç de l'ala superior. t = 1,20.

Es calcula la tensió crítica:

$$\sigma_{cr,s}(0{,}75) = \frac{4{,}2 \cdot k_w \cdot E}{A_s} \cdot \sqrt{\frac{I_s \cdot t^3}{4 \cdot {b_p}^2 \cdot (2 \cdot b_p + 3 \cdot b_s)}} = 780{,}90\,MPa$$

$$\sigma_{cr,s}(1{,}00) = \frac{4{,}2 \cdot k_w \cdot E}{A_s} \cdot \sqrt{\frac{I_s \cdot t^3}{4 \cdot {b_p}^2 \cdot (2 \cdot b_p + 3 \cdot b_s)}} = 621{,}40\,MPa$$

$$\sigma_{cr,s}(1{,}20) = \frac{4{,}2 \cdot k_w \cdot E}{A_s} \cdot \sqrt{\frac{I_s \cdot t^3}{4 \cdot {b_p}^2 \cdot (2 \cdot b_p + 3 \cdot b_s)}} = 765{,}30\,MPa$$

$$k_w = k_{w0} = 1{,}48$$

$$k_{w0} = \sqrt{\frac{s_w + 2 \cdot b_d}{s_w + 0{,}5 \cdot b_d}} = 1{,}48$$

$$l_b(0{,}75) = 3{,}07 \cdot \sqrt[4]{\frac{I_s \cdot {b_p}^2 \cdot (2 \cdot b_p + 3 \cdot b_s)}{t^3}} = 317{,}37\,mm$$

$$l_b(1{,}00) = 3{,}07 \cdot \sqrt[4]{\frac{I_s \cdot {b_p}^2 \cdot (2 \cdot b_p + 3 \cdot b_s)}{t^3}} = 280{,}14\,mm$$

$$l_b(1{,}20) = 3{,}07 \cdot \sqrt[4]{\frac{I_s \cdot {b_p}^2 \cdot (2 \cdot b_p + 3 \cdot b_s)}{t^3}} = 258{,}98\,mm$$

L’alçada inclinada de l’ànima és $s_w=b_{p3}$. També s’utilitzen les longituds segons la Fig. A.3, el moment d’inèrcia i secció eficaç anteriors.

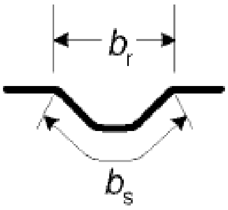

Fig. A.3. Figura 5.11 de EN 1993-1-3:2006 [2].

Es calcula el valor de l’esveltesa relativa i posteriorment un factor reductor:

$$\overline{\lambda_d}(0{,}75) = \sqrt{\frac{f_{yb}}{\sigma_{cr,s}}} = 0{,}89$$

$$\overline{\lambda_d}(1{,}00) = \sqrt{\frac{f_{yb}}{\sigma_{cr,s}}} = 0{,}78$$

$$\overline{\lambda_d}(1{,}20) = \sqrt{\frac{f_{yb}}{\sigma_{cr,s}}} = 0{,}71$$

$$\chi_d(0{,}75) = 1{,}47 - 0{,}723 \cdot \overline{\lambda_d} = 0{,}83$$

$$\chi_d(1{,}00) = 1{,}47 - 0{,}723 \cdot \overline{\lambda_d} = 0{,}91$$

$$\chi_d(1{,}20) = 1{,}47 - 0{,}723 \cdot \overline{\lambda_d} = 0{,}96$$

Finalment, el gruix reduït de la part de l’ala superior on està el rigiditzador i la part plana que té contacte directe segons la Fig. A.4.

$$t_{red}(0{,}75) = \chi_d \cdot t = 0{,}59\ mm$$

$$t_{red}(1{,}00) = \chi_d \cdot t = 0{,}87\ mm$$

$$t_{red}(1{,}20) = \chi_d \cdot t = 1{,}11\ mm$$

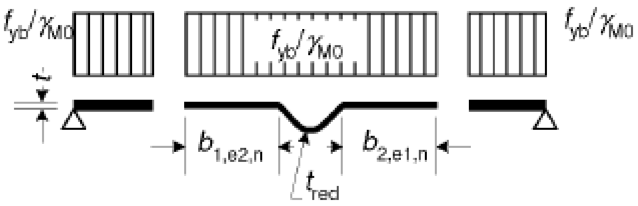

Fig. A.4. Figura 5.10 de EN 1993-1-3:2006 [2].

A.1.1.2. Ànima

Es calcula el gruix reduït necessari per tenir en compte les perforacions que existeixen en l'ànima segons:

$$t_{b,eff}(0{,}75) = t \cdot \sqrt[3]{1{,}18 \cdot \left(1 - \frac{d}{a}\right)} = 0{,}66\ mm$$

$$t_{b,eff}(1{,}00) = t \cdot \sqrt[3]{1{,}18 \cdot \left(1 - \frac{d}{a}\right)} = 0{,}89\ mm$$

$$t_{b,eff}(1{,}20) = t \cdot \sqrt[3]{1{,}18 \cdot \left(1 - \frac{d}{a}\right)} = 1{,}07\ mm$$

El diàmetre dels forats és de $d = 0{,}40\ mm$ i la distancia lliure entre ells de $a = 12{,}00\ mm$.

Abans de la fallada de la secció es pot apreciar una petita plastificació parcial en la zona traccionada de l'ànima, mentre que la resta de la secció encara té un comportament elàstic.

En la primera aproximació de l'eix neutre s'assumeix que tota la l'ànima és completament efectiva i que la part del rigiditzador i la part plana de l'ala superior tenen la mateixa tensió com es mostra en la Fig. A.5.

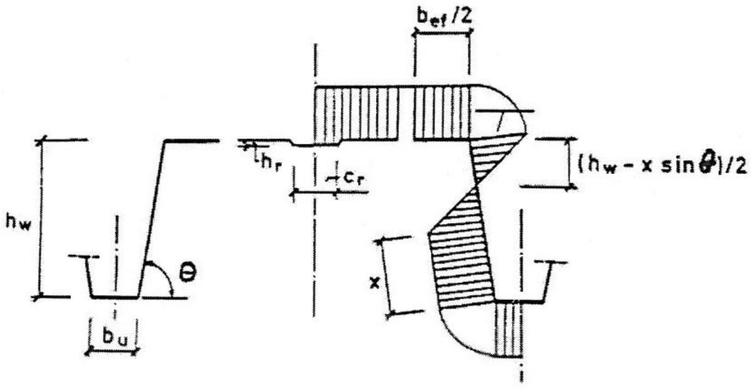

Fig. A.5. Primera aproximació de l'eix neutre efectiu.

Aplicant les condicions d'equilibri trobem, gràcies a un procés iteratiu, una primera aproximació de x i la tensió real (σ_r) que té el rigiditzador de l'ala superior (Taula A.6):

$$\frac{f_{yb}}{\gamma_{M0}} \cdot (A_{coner\,1inf} + A_1 + A_{corner\,1sup} + A_{21} + A_{22} + A_{corner\,2sup}) = \frac{f_{yb}}{\gamma_{M0}} \cdot (A_{coner\,2inf} + A_4)$$

$$\sigma_r = \frac{f_{yb}}{\gamma_{M0}} \cdot \left(1 - 2 \cdot \frac{h_r}{h - x \cdot \sin(\theta)}\right)$$

		Iteració 0	Iteració 1	Iteració 2	Iteració 3
t = 0,75 mm	**x (mm)**	5,64	2,58	2,65	2,64
	σ_r (MPa)	264,81	270,67	270,55	270,55
t = 1,00 mm	**x (mm)**	13,72	9,92	10,07	10,07
	σ_r (MPa)	248,37	256,95	256,64	256,64
t = 1,20 mm	**x (mm)**	16,97	15,11	15,22	15,22
	σ_r (MPa)	240	245,92	244,64	244,64

Taula A.6. Resultats iteratius de la dimensió x.

Per calcular longitud no eficaç de l'ànima s_{Neff}, s'utilitzen les longituds equivalents $s_{eff,1}$ i $s_{eff,2}$. En quan a la longitud no eficaç de l'ànima s'ha de diferencia entre les usades en el càlcul del mòdul resistent i les usades en el càlcul del moment d'inèrcia.

$$s_{eff,0}(0{,}75) = 0{,}95 \cdot t \cdot \sqrt{\frac{E}{\gamma_{M0} \cdot f_{yb}}} = 11{,}76\ mm$$

$$s_{eff,0}(1{,}00) = 0{,}95 \cdot t \cdot \sqrt{\frac{E}{\gamma_{M0} \cdot f_{yb}}} = 15{,}90\ mm$$

$$s_{eff,0}(1{,}20) = 0{,}95 \cdot t \cdot \sqrt{\frac{E}{\gamma_{M0} \cdot f_{yb}}} = 19{,}21\ mm$$

$$s_{eff,1}(0{,}75) = s_{eff,0} = 11{,}76\ mm$$

$$s_{eff,1}(1{,}00) = s_{eff,0} = 15{,}90\ mm$$

$$s_{eff,1}(1{,}20) = s_{eff,0} = 19{,}21\ mm$$

$$s_{eff,n}(0{,}75) = 1{,}5 \cdot s_{eff,0} = 17{,}63\ mm$$

$$s_{eff,n}(1{,}00) = 1{,}5 \cdot s_{eff,0} = 23{,}84\ mm$$

$$s_{eff,n}(1{,}20) = 1{,}5 \cdot s_{eff,0} = 28{,}81\ mm$$

Mòdul resistent

$$s_{Neff}(0{,}75) = s_n - \left(s_{eff,1} + s_{eff,n}\right) = -1{,}03\ mm \geq 0$$

$$s_{Neff}(1{,}00) = s_n - \left(s_{eff,1} + s_{eff,n}\right) = -14{,}68\ mm \geq 0$$

$$s_{Neff}(1{,}20) = s_n - \left(s_{eff,1} + s_{eff,n}\right) = -25{,}23\ mm \geq 0$$

Moment d'inèrcia

		Iteració 0	**Iteració 1**
t = 0,75 mm	**s_{Neff} (mm)**	-9,32 < 0	-6,33 < 0
t = 1,00 mm	**s_{Neff} (mm)**	-22,34 < 0	-21,06 < 0
t = 1,20 mm	**s_{Neff} (mm)**	-31,09 < 0	-31,22 < 0

Taula A.7. Resultats iteratius de la longitud no eficaç de l'ànima.

A.1.1.3. Resultats

Els resultats pel càlcul del mòdul resistent són els següents:

Element	**L_i (mm)**	**t_{eff} (mm)**	**A_i (mm^2)**	**σ_r (N/mm^2)**	**z (mm)**	**M (kN·mm)**
Corner 1inf	2,30	0,59	1,33	270,55	7,81	2818,65
1	10,50	0,59	6,16	270,55	4,00	7976,02
Corner 1sup	2,30	0,59	1,33	323,78	0,19	95,10
21	11,30	0,59	6,65	377,00	0,00	0,00
22	10,70	0,71	7,58	377,00	0,00	0,00
Corner 2sup	3,60	0,71	2,57	377,00	0,48	463,46
31	16,10	0,66	10,53	377,00	9,44	37478,94
32	16,10	0,66	10,53	377,00	47,22	187394,71
33	2,60	0,66	1,73	377,00	57,83	37788,22
Corner 2inf	3,60	0,71	2,57	377,00	58,52	56778,20
4	27,00	0,71	19,16	377,00	59,00	426210,31
TOTAL			70,1		252,50	**659,34**

Taula A.8. Resultats del moment. t = 0,75 mm.

Element	**L_i (mm)**	**t_{eff} (mm)**	**A_i (mm^2)**	**σ_r (N/mm^2)**	**z (mm)**	**M (kN·mm)**
Corner 1inf	2,35	0,87	2,04	256,64	7,80	4093,98
1	10,36	0,87	9,02	316,82	4,00	11435,02
Corner 1sup	2,35	0,87	2,04	377,00	0,20	151,18
21	13,93	0,87	12,13	377,00	0,00	0,00
22	13,29	0,96	12,76	377,00	0,00	0,00
Corner 2sup	3,76	0,96	3,61	377,00	0,50	674,22
31	14,20	0,89	12,59	377,00	8,35	39640,69
32	14,20	0,89	12,59	377,00	41,77	198203,47
33	10,07	0,89	8,92	377,00	54,56	183514,64
Corner 2inf	3,76	0,96	3,61	377,00	58,50	79606,61
4	26,91	0,96	25,84	377,00	59,00	574683,73
TOTAL			105,15		242,68	**980,01**

Taula A.9. Resultats del moment. t = 1,00 mm.

Element	**L_i (mm)**	**t_{eff} (mm)**	**A_i (mm^2)**	**σ_r (N/mm^2)**	**z (mm)**	**M (kN·mm)**
Corner 1inf	2,42	1,11	2,69	244,64	7,80	5129,22
1	10,29	1,11	11,46	310,82	4,00	14246,10
Corner 1sup	2,42	1,11	2,69	377,00	0,20	204,56
21	14,63	1,11	16,28	377,00	0,00	0,00
22	13,97	1,16	16,21	377,00	0,00	0,00
Corner 2sup	3,87	1,16	4,49	377,00	0,51	862,17
31	12,92	1,07	13,83	377,00	7,60	39609,99
32	12,92	1,07	13,83	377,00	37,98	198049,94
33	15,22	1,07	16,29	377,00	52,29	321217,06
Corner 2inf	3,87	1,16	4,49	377,00	58,49	98931,36
4	26,85	1,16	31,15	377,00	59,00	692862,24
TOTAL			**133,40**		235,86	**1251,01**

Taula A.10. Resultats del moment. t = 1,20 mm.

	t = 0,75 mm	**t = 1,00 mm**	**t = 1,20 mm**
$M_{el,Rd,eff}$ (kN·m/m)	6,43	9,56	12,20
$W_{res,eff}$ (mm^3/m)	17062,54	25361,02	32373,90

Taula A.11. Resultats del mòdul resistent.

Els resultats iteratius pel càlcul del moment d'inèrcia resistent són els següents:

Element	**L_i (mm)**	**t_{eff} (mm)**	**A_i (mm^2)**	**z (mm)**	**S_i (mm^3)**	**z_0 (mm)**
Corner 1inf	2,30	0,59	1,33	51,19	68,28	-20,60
1	10,50	0,59	6,16	55,00	338,72	-20,79
Corner 1sup	2,30	0,59	1,33	58,81	78,44	-24,60
21	11,30	0,59	6,65	59,00	392,32	-28,41
22	10,70	0,71	7,58	59,00	447,00	-28,60
Corner 2sup	3,60	0,71	2,57	58,52	150,61	-28,60
3	62,90	0,66	41,20	29,50	1215,40	-28,13
Corner 2inf	3,60	0,71	2,57	0,48	1,23	0,90
4	27,00	0,71	19,16	0,00	0,00	29,92
TOTAL			**88,63**		2692,00	**30,40**

Taula A.12. Resultats de la iteració 0 de l'eix neutre. t = 0,75 mm.

Element	**L_i (mm)**	**t_{eff} (mm)**	**A_i (mm^2)**	**z (mm)**	**S_i (mm^3)**	**z_0 (mm)**	**I_i (mm^4)**
Corner 1inf	2,30	0,59	1,33	51,19	68,28	-20,60	694,82
1	10,50	0,59	6,16	55,00	338,72	-20,79	3749,76
Corner 1sup	2,30	0,59	1,33	58,81	78,44	-24,60	1297,60
21	11,30	0,59	6,65	59,00	392,32	-28,41	5440,25
22	10,70	0,71	7,58	59,00	447,00	-28,60	6198,57
Corner 2sup	3,60	0,71	2,57	58,52	150,61	-28,60	1271,38
3	62,90	0,66	41,20	29,50	1215,40	-28,13	10590,14
Corner 2inf	3,60	0,71	2,57	0,48	1,23	0,90	1438,79
4	27,00	0,71	19,16	0,00	0,00	29,92	17705,94
TOTAL			**88,63**		2692,00	**30,40**	**48387,25**

Taula A.13. Resultats de la iteració 1 de l'eix neutre. t = 0,75 mm.

Element	**L_i (mm)**	**t_{eff} (mm)**	**A_i (mm^2)**	**z (mm)**	**S_i (mm^3)**	**z_0 (mm)**
Corner 1inf	2,30	0,87	2,04	51,20	104,65	-19,28
1	10,40	0,87	9,02	55,00	496,28	-23,08
Corner 1sup	2,30	0,87	2,04	58,80	120,21	-26,88
21	13,90	0,87	12,13	59,00	715,44	-27,08
22	13,30	0,96	12,76	59,00	752,80	-27,08
Corner 2sup	3,80	0,96	3,61	58,50	211,16	-26,59
3	62,70	0,89	55,57	29,50	1639,43	2,42
Corner 2inf	3,80	0,96	3,61	0,50	1,79	31,42
4	26,90	0,96	25,84	0,00	0,00	31,92
TOTAL			**126,63**		4041,877	**31,92**

Taula A.14. Resultats de la iteració 0 de l'eix neutre. t = 1,00 mm.

Element	**L_i (mm)**	**t_{eff} (mm)**	**A_i (mm^2)**	**z (mm)**	**S_i (mm^3)**	**z_0 (mm)**	**I_i (mm^4)**
Corner 1inf	2,30	0,87	2,04	51,20	104,65	-19,28	837,68
1	10,40	0,87	9,02	55,00	496,28	-23,08	4838,96
Corner 1sup	2,30	0,87	2,04	58,80	120,21	-26,88	1629,32
21	13,90	0,87	12,13	59,00	715,44	-27,08	8893,91
22	13,30	0,96	12,76	59,00	752,80	-27,08	9358,57
Corner 2sup	3,80	0,96	3,61	58,50	211,16	-26,59	1593,24
3	62,70	0,89	55,57	29,50	1639,43	2,42	14497,85
Corner 2inf	3,80	0,96	3,61	0,50	1,79	31,42	2225,84
4	26,90	0,96	25,84	0,00	0,00	31,92	26324,68
TOTAL			**126,63**		4041,877	**31,92**	**70200,05**

Taula A.15. Resultats de la iteració 1 de l'eix neutre. t = 1,00 mm.

Element	**L_i (mm)**	**t_{eff} (mm)**	**A_i (mm^2)**	**z (mm)**	**S_i (mm^3)**	**z_0 (mm)**
Corner 1inf	2,40	1,10	2,67	51,20	136,60	-18,75
1	10,30	1,10	11,37	55,00	625,37	-22,54
Corner 1sup	2,40	1,10	2,67	58,80	156,87	-26,34
21	14,60	1,10	16,16	59,00	953,15	-26,54
22	14,00	1,16	16,21	59,00	956,15	-26,54
Corner 2sup	3,90	1,16	4,49	58,49	262,42	-26,03
3	62,60	1,07	67,02	29,50	1977,20	2,96
Corner 2inf	3,90	1,16	4,49	0,51	2,29	31,95
4	26,90	1,16	31,15	0,00	0,00	32,46
TOTAL			**156,21**		5070,03	**32,46**

Taula A.16. Resultats de la iteració 0 de l'eix neutre. t = 1,20 mm.

Element	**L_i (mm)**	**t_{eff} (mm)**	**A_i (mm^2)**	**z (mm)**	**S_i (mm^3)**	**z_0 (mm)**	**I_i (mm^4)**
Corner 1inf	2,40	1,10	2,67	51,20	136,60	-18,75	984,68
1	10,30	1,10	11,37	55,00	625,37	-22,54	5818,72
Corner 1sup	2,40	1,10	2,67	58,80	156,87	-26,34	1944,41
21	14,60	1,10	16,16	59,00	953,15	-26,54	11384,36
22	14,00	1,16	16,21	59,00	956,15	-26,54	11420,39
Corner 2sup	3,90	1,16	4,49	58,49	262,42	-26,03	1899,22
3	62,60	1,07	67,02	29,50	1977,20	2,96	17613,30
Corner 2inf	3,90	1,16	4,49	0,51	2,29	31,95	2859,65
4	26,90	1,16	31,15	0,00	0,00	32,46	32815,96
TOTAL			**156,21**		5070,03	**32,46**	**86740,68**

Taula A.17. Resultats de la iteració 1 de l'eix neutre. t = 1,20 mm.

	t = 0,75 mm	**t = 1,00 mm**	**t = 1,20 mm**
$I_{EN,eff}$ (mm^4/m)	472070,74	684878,57	846250,52

Taula A.18. Resultats del moment d'inèrcia resistent.

A.1.2. Moment negatiu

A.1.2.1. Ànima

Es calcula el gruix reduït necessari per tenir en compte les perforacions que existeixen en l'ànima segons:

$$t_{b,eff}(0{,}75) = t \cdot \sqrt[3]{1{,}18 \cdot \left(1 - \frac{d}{a}\right)} = 0{,}66\ mm$$

$$t_{b,eff}(1{,}00) = t \cdot \sqrt[3]{1{,}18 \cdot \left(1 - \frac{d}{a}\right)} = 0{,}89\ mm$$

$$t_{b,eff}(1{,}20) = t \cdot \sqrt[3]{1{,}18 \cdot \left(1 - \frac{d}{a}\right)} = 1{,}07\ mm$$

El diàmetre dels forats és de $d = 0{,}40\ mm$ i la distancia lliure entre ells de $a = 12{,}00\ mm.$

Per calcular longitud no eficaç de l'ànima s_{Neff}, s'utilitzen les longituds equivalents $s_{eff,1}$ i $s_{eff,2}$:

$$s_{eff,0}(0{,}75) = 0{,}95 \cdot t \cdot \sqrt{\frac{E}{\gamma_{M0} \cdot f_{yb}}} = 14{,}70\ mm$$

$$s_{eff,0}(1{,}00) = 0{,}95 \cdot t \cdot \sqrt{\frac{E}{\gamma_{M0} \cdot f_{yb}}} = 19{,}87\ mm$$

$$s_{eff,0}(1{,}20) = 0{,}95 \cdot t \cdot \sqrt{\frac{E}{\gamma_{M0} \cdot f_{yb}}} = 24{,}01\ mm$$

$$s_{eff,1}(0{,}75) = s_{eff,0} = 14{,}70\ mm$$

$$s_{eff,1}(1{,}00) = s_{eff,0} = 19{,}87\ mm$$

$$s_{eff,1}(1{,}20) = s_{eff,0} = 24{,}01\ mm$$

$$s_{eff,n}(0{,}75) = 1{,}5 \cdot s_{eff,0} = 22{,}04\ mm$$

$$s_{eff,n}(1{,}00) = 1{,}5 \cdot s_{eff,0} = 29{,}80\ mm$$

$$s_{eff,n}(1{,}20) = 1{,}5 \cdot s_{eff,0} = 36{,}01\ mm$$

		Iteració 0	Iteració 1	Iteració 2
t = 0,75 mm	**s_{Neff} (mm)**	-1,29 < 0	5,37	5,85
t = 1,00 mm	**s_{Neff} (mm)**	-14,30 < 0	-8,40 < 0	
t = 1,20 mm	**s_{Neff} (mm)**	-24,70 < 0	-19,33 < 0	

Taula A.19. Resultats iteratius de la longitud no eficaç de l'ànima.

A.1.2.2. Ala inferior

Mitjançant el procediment detallat en l'Eurocodi 3 es pot trobar l'esveltesa relativa pels diferents gruixos.

$$\overline{\lambda_p}(0{,}75) = \sqrt{\frac{f_{yb}}{\sigma_{cr}}} = \frac{\frac{\bar{b}}{t}}{\left(28{,}4 \cdot \varepsilon \cdot k_\sigma^{\frac{1}{2}}\right)} = 1{,}80$$

$$\overline{\lambda_p}(1{,}00) = \sqrt{\frac{f_{yb}}{\sigma_{cr}}} = \frac{\frac{\bar{b}}{t}}{\left(28{,}4 \cdot \varepsilon \cdot k_\sigma^{\frac{1}{2}}\right)} = 1{,}33$$

$$\overline{\lambda_p}(1{,}20) = \sqrt{\frac{f_{yb}}{\sigma_{cr}}} = \frac{\frac{\bar{b}}{t}}{\left(28{,}4 \cdot \varepsilon \cdot k_\sigma^{\frac{1}{2}}\right)} = 1{,}10$$

$$\varepsilon = \sqrt{\frac{235}{f_{yb}}} = 0{,}79$$

El factor de vinclament utilitzat és $k_\sigma = 4$ i $\bar{b} = b_{p2}$.

Ja es pot calcular el factor reductor ρ que varia segons el material utilitzat. En el cas que ens pertoca, per l'acer, s'utilitzarà la següent formula:

$$\rho\ (0{,}75) = \frac{1 - 0{,}55 \cdot \frac{(3+\psi)}{\overline{\lambda_p}}}{\overline{\lambda_p}} = 0{,}49$$

$$\rho\ (1{,}00) = \frac{1 - 0{,}55 \cdot \frac{(3+\psi)}{\overline{\lambda_p}}}{\overline{\lambda_p}} = 0{,}63$$

$$\rho\,(1{,}20) = \frac{1 - 0{,}55 \cdot \frac{(3+\psi)}{\overline{\lambda_p}}}{\overline{\lambda_p}} = 0{,}73$$

El rati de tensions (σ_2/σ_1) és $\psi=1$.

Aquest factor en indica si cal considerar que la regió $\bar{b}$ en tota la seva longitud és o no efectiva. Per tant la longitud eficaç de la zona plana de l'ala és:

$$b_{eff}(0{,}75) = \rho \cdot \bar{b} = 13{,}98\ mm$$

$$b_{eff}(1{,}00) = \rho \cdot \bar{b} = 17{,}97\ mm$$

$$b_{eff}(1{,}20) = \rho \cdot \bar{b} = 20{,}82\ mm$$

La longitud utilitzada és $\bar{b} = b_{p2}$

A.1.2.3. Resultats

Els resultats iteratius pel càlcul del moment d'inèrcia resistent i el mòdul resistent són els següents:

Element	L_i (mm)	t_{eff} (mm)	A_i (mm^2)	z (mm)	S_i (mm^3)	z_0 (mm)
Corner 1inf	2,30	0,71	1,61	7,81	12,55	12,27
1	10,50	0,71	7,42	4,00	29,69	16,08
Corner 1sup	2,30	0,71	1,61	0,19	0,30	19,89
2	28,80	0,71	20,46	0,00	0,00	20,08
Corner 2sup	3,60	0,71	2,57	0,48	1,23	19,61
3	62,90	0,66	41,20	29,50	1215,40	-9,42
Corner 2inf	3,60	0,71	2,57	58,52	150,61	-38,44
4	5,30	0,71	3,74	59,00	220,49	-38,92
TOTAL			**81,18**		1630,27	**20,08**

Taula A.20. Resultats de la iteració 0 de l'eix neutre. t = 0,75 mm.

Element	L_i (mm)	t_{eff} (mm)	A_i (mm^2)	z (mm)	S_i (mm^3)	z_0 (mm)
Corner 1inf	2,30	0,71	1,61	7,81	12,55	11,85
1	10,50	0,71	7,42	4,00	29,69	15,66
Corner 1sup	2,30	0,71	1,61	0,19	0,30	19,47
2	28,80	0,71	20,46	0,00	0,00	19,66
Corner 2sup	3,60	0,71	2,57	0,48	1,23	19,18
3	57,49	0,66	37,68	29,50	1111,64	-9,84
Corner 2inf	3,60	0,71	2,57	58,52	150,61	-38,87
4	5,30	0,71	3,74	59,00	220,49	-39,34
TOTAL			**77,66**		1526,51	**19,66**

Taula A.21. Resultats de la iteració 1 de l'eix neutre. t = 0,75 mm.

Element	L_i (mm)	t_{eff} (mm)	A_i (mm^2)	z (mm)	S_i (mm^3)	z_0 (mm)	I_i (mm^4)
Corner 1inf	2,30	0,71	1,61	7,81	12,55	11,81	224,00
1	10,50	0,71	7,42	4,00	29,69	15,62	1836,38
Corner 1sup	2,30	0,71	1,61	0,19	0,30	19,43	606,61
2	28,80	0,71	20,46	0,00	0,00	19,62	7872,33
Corner 2sup	3,60	0,71	2,57	0,48	1,23	19,14	588,72
3	57,01	0,66	37,37	29,50	1102,29	-9,88	11525,59
Corner 2inf	3,60	0,71	2,57	58,52	150,61	-38,91	2432,88
4	5,30	0,71	3,74	59,00	220,49	-39,38	5796,73
TOTAL			**77,34**		1517,16	**19,62**	**30883,24**

Taula A.22. Resultats de la iteració 2 de l'eix neutre. t = 0,75 mm.

Element	L_i (mm)	t_{eff} (mm)	A_i (mm^2)	z (mm)	S_i (mm^3)	z_0 (mm)
Corner 1inf	2,30	0,96	2,25	7,80	17,59	12,95
1	10,40	0,96	9,95	4,00	39,80	16,75
Corner 1sup	2,40	0,96	2,25	0,20	0,44	20,55
2	28,70	0,96	27,54	0,00	0,00	20,75
Corner 2sup	3,80	0,96	3,61	0,50	1,79	20,25
3	62,70	0,89	55,57	29,50	1639,43	-8,75
Corner 2inf	3,80	0,96	3,61	58,50	211,16	-37,75
4	7,20	0,96	6,91	59,00	407,65	-38,25
TOTAL			**111,71**		2317,87	**20,75**

Taula A.23. Resultats de la iteració 0 de l'eix neutre. t = 1,00 mm.

Element	**L_i (mm)**	**t_{eff} (mm)**	**A_i (mm^2)**	**z (mm)**	**S_i (mm^3)**	**z_0 (mm)**	**I_i (mm^4)**
Corner 1inf	2,30	0,96	2,25	7,80	17,59	12,95	377,80
1	10,40	0,96	9,95	4,00	39,80	16,75	2826,84
Corner 1sup	2,40	0,96	2,25	0,20	0,44	20,55	952,29
2	28,70	0,96	27,54	0,00	0,00	20,75	11861,69
Corner 2sup	3,80	0,96	3,61	0,50	1,79	20,25	924,75
3	62,70	0,89	55,57	29,50	1639,43	-8,75	18427,70
Corner 2inf	3,80	0,96	3,61	58,50	211,16	-37,75	3213,13
4	7,20	0,96	6,91	59,00	407,65	-38,25	10109,49
TOTAL			**111,71**		2317,87	**20,75**	**48693,70**

Taula A.24. Resultats de la iteració 1 de l'eix neutre. t = 1,00 mm.

Element	**L_i (mm)**	**t_{eff} (mm)**	**A_i (mm^2)**	**z (mm)**	**S_i (mm^3)**	**z_0 (mm)**
Corner 1inf	2,40	1,16	2,80	7,80	21,85	13,41
1	10,30	1,16	11,94	4,00	47,77	17,21
Corner 1sup	2,40	1,16	2,80	0,20	0,57	21,01
2	28,60	1,16	33,17	0,00	0,00	21,21
Corner 2sup	3,90	1,16	4,49	0,51	2,29	20,70
3	62,60	1,07	67,02	29,50	1977,20	-8,29
Corner 2inf	3,90	1,16	4,49	58,49	262,42	-37,28
4	8,60	1,16	9,94	59,00	586,56	-37,79
TOTAL			**136,66**		2898,64	**21,21**

Taula A.25. Resultats de la iteració 0 de l'eix neutre. t = 1,20 mm.

Element	**L_i (mm)**	**t_{eff} (mm)**	**A_i (mm^2)**	**z (mm)**	**S_i (mm^3)**	**z_0 (mm)**	**I_i (mm^4)**
Corner 1inf	2,40	1,16	2,80	7,80	21,85	13,41	504,10
1	10,30	1,16	11,94	4,00	47,77	17,21	3579,37
Corner 1sup	2,40	1,16	2,80	0,20	0,57	21,01	1236,80
2	28,60	1,16	33,17	0,00	0,00	21,21	14928,51
Corner 2sup	3,90	1,16	4,49	0,51	2,29	20,70	1200,81
3	62,60	1,07	67,02	29,50	1977,20	-8,29	21632,69
Corner 2inf	3,90	1,16	4,49	58,49	262,42	-37,28	3894,14
4	8,60	1,16	9,94	59,00	586,56	-37,79	14197,83
TOTAL			**136,66**		2898,64	**21,21**	**61174,26**

Taula A.26. Resultats de la iteració 1 de l'eix neutre. t = 1,20 mm.

	t = 0,75 mm	**t = 1,00 mm**	**t = 1,20 mm**
$I_{EN,eff}$ (mm^4/m)	301299,94	475060,48	596822,05
$W_{res,eff}$ (mm^3/m)	7650,38	12419,84	15793,56

Taula A.27. Resultats del moment d'inèrcia resistent.

A.2. Perfil PLAIN

A.2.1. Moment positiu

A.2.1.1. Ala superior

Mitjançant el procediment detallat en l'Eurocodi 3 es pot trobar l'esveltesa relativa pels diferents gruixos.

$$\overline{\lambda_p} = \sqrt{\frac{f_{yb}}{\sigma_{cr}}} = \frac{\frac{\bar{b}}{t}}{\left(28{,}4 \cdot \varepsilon \cdot k_{\sigma}^{\frac{1}{2}}\right)} = 0{,}99$$

$$\varepsilon = \sqrt{\frac{235}{f_{yb}}} = 0{,}79$$

El factor de vinclament utilitzat és $k_\sigma = 4$ i $\bar{b} = b_{p2}$.

Ja es pot calcular el factor reductor ρ que varia segons el material utilitzat. En el cas que ens pertoca, per l'acer, s'utilitzarà la següent formula:

$$\rho = \frac{1 - 0{,}55 \cdot \frac{(3+\psi)}{\overline{\lambda_p}}}{\overline{\lambda_p}} = 0{,}78$$

El rati de tensions (σ_2/σ_1) és $\psi=1$.

Aquest factor en indica si cal considerar que la regió $\bar{b}$ en tota la seva longitud és o no efectiva. Per tant la longitud eficaç de la zona plana de l'ala és:

$$b_{eff} = \rho \cdot \bar{b} = 24{,}80\, mm$$

La longitud utilitzada és $\bar{b} = b_{p2}$

S'obté l'àrea eficaç de la part dels rigiditzadors de l'ala superior. S'utilitza el procediment indicat en la normativa EN 1993-1-3:2006 [2]. Primer es calcula una secció eficaç (Taula A.28) utilitzant les especificacions de la Fig. A.6.

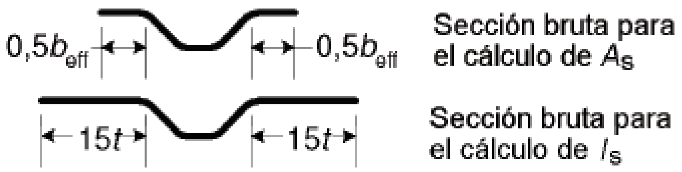

Fig. A.6. Figura 5.11 de EN 1993-1-3:2006 [2].

Element	L_i (mm)	A_i (mm^2)
Part plana (Fig. A.6)	11,29	8,01
Corner 1sup	2,26	1,61
1	10,45	7,42
Corner 1inf	2,26	1,61
Corner 1inf	2,26	1,61
1	10,45	7,42
Corner 1sup	2,26	1,61
Part plana (Fig. A.6)	11,29	8,01
TOTAL		**37,30**

Taula A.28. Primer càlcul de la secció eficaç de l'ala superior.

També s'obté una primera inèrcia eficaç (Taula A.29) segons la Fig. A.6.

Element	L_i (mm)	A_i (mm^2)	Z (mm)	S_i (mm^3)	z_0 (mm)	I_i (mm^4)
Part plana (Fig. A.6)	9,54	6,77	0,00	0,00	2,48	41,90
Corner 1sup	2,30	1,61	0,19	0,30	2,29	8,43
1	10,50	7,42	4,00	29,69	-1,52	43,73
Corner 1inf	2,30	1,61	8,19	13,16	-5,71	52,41
Corner 1inf	2,30	1,61	8,19	13,16	-5,71	52,41
1	10,5	7,42	4,00	29,69	-1,52	43,73
Corner 1sup	2,30	1,61	0,19	0,30	2,29	8,43
Part plana (Fig. A.6)	9,54	6,77	0,00	0,00	2,48	41,90
TOTAL		34,82		86,30	2,48	**292,94**

Taula A.29. Primer càlcul del moment inèrcia eficaç de l'ala superior.

Es calcula la tensió crítica:

$$\sigma_{cr,s} = \frac{4{,}2 \cdot k_w \cdot E}{A_s} \cdot \sqrt{\frac{I_s \cdot t^3}{4 \cdot {b_p}^2 \cdot (2 \cdot b_p + 3 \cdot b_s)}} = 480{,}90\ MPa$$

$$k_w = k_{w0} = 1{,}48$$

$$k_{w0} = \sqrt{\frac{s_w + 2 \cdot b_d}{s_w + 0{,}5 \cdot b_d}} = 1{,}48$$

$$l_b = 3{,}07 \cdot \sqrt[4]{\frac{I_s \cdot {b_p}^2 \cdot (2 \cdot b_p + 3 \cdot b_s)}{t^3}} = 317{,}37\ mm$$

L'alçada inclinada de l'ànima és s_w=b_{p3}. També s'utilitzen les longituds segons la Fig. A.7, el moment d'inèrcia i secció eficaç anteriors.

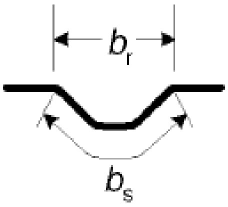

Fig. A.7. Figura 5.11 de EN 1993-1-3:2006 [2].

Es calcula el valor de l'esveltesa relativa i posteriorment un factor reductor:

$$\overline{\lambda_d} = \sqrt{\frac{f_{yb}}{\sigma_{cr,s}}} = 0{,}89$$

$$\chi_d = 1{,}47 - 0{,}723 \cdot \overline{\lambda_d} = 0{,}83$$

Finalment, el gruix reduït de la part de l'ala superior on està el rigiditzador i la part plana que té contacte directe segons la Fig. A.8.

$$t_{red} = \chi_d \cdot t = 0{,}59\ mm$$

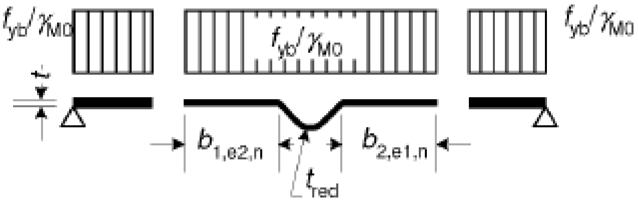

Fig. A.8. Figura 5.10 de EN 1993-1-3:2006 [2].

A.2.1.2. Ànima

Abans de la fallada de la secció es pot apreciar una petita plastificació parcial en la zona traccionada de l'ànima, mentre que la resta de la secció encara té un comportament elàstic.

En la primera aproximació de l'eix neutre s'assumeix que tota la l'ànima és completament efectiva i que la part del rigiditzador i la part plana de l'ala superior tenen la mateixa tensió com es mostra en la Fig. A.9.

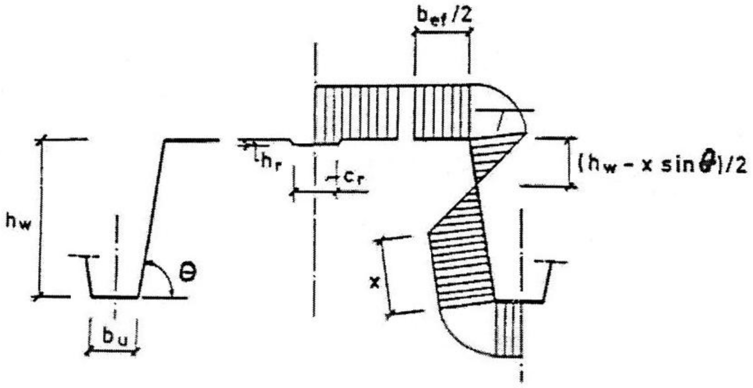

Fig. A.9. Primera aproximació de l'eix neutre efectiu.

Aplicant les condicions d'equilibri trobem, gràcies a un procés iteratiu, una primera aproximació de x i la tensió real (σr) que té el rigiditzador de l'ala superior (Taula A.30):

$$\frac{f_{yb}}{\gamma_{M0}} \cdot (A_{coner\,1inf} + A_1 + A_{corner\,1sup} + A_{21} + A_{22} + A_{corner\,2sup}) = \frac{f_{yb}}{\gamma_{M0}} \cdot (A_{coner\,2inf} + A_4)$$

$$\sigma_r = \frac{f_{yb}}{\gamma_{M0}} \cdot \left(1 - 2 \cdot \frac{h_r}{h - x \cdot \sin(\theta)}\right)$$

	Iteració 0	**Iteració 1**	**Iteració 2**	**Iteració 3**
x (mm)	5,48	2,59	2,65	2,64
σ_r (MPa)	266,64	270,65	270,55	270,55

Taula A.30. Resultats iteratius de la dimensió x.

Per calcular longitud no eficaç de l'ànima s_{Neff}, s'utilitzen les longituds equivalents $s_{eff,1}$ i $s_{eff,2}$. En quan a la longitud no eficaç de l'ànima s'ha de diferencia entre les usades en el càlcul del mòdul resistent i les usades en el càlcul del moment d'inèrcia.

$$s_{eff,0} = 0{,}95 \cdot t \cdot \sqrt{\frac{E}{\gamma_{M0} \cdot f_{yb}}} = \ 12{,}74\,mm$$

$$s_{eff,1} = s_{eff,0} = 12{,}74\,mm$$

$$s_{eff,n} = 1{,}5 \cdot s_{eff,0} = 19{,}10\,mm$$

Mòdul resistent

$$s_{Neff} = \ s_n - \left(s_{eff,1} + s_{eff,n}\right) = -3{,}50\,mm \geq 0$$

Moment d'inèrcia

	Iteració 0	**Iteració 1**
s_{Neff} (mm)	-11,87 < 0	-9,35 < 0

Taula A.31. Resultats iteratius de la longitud no eficaç de l'ànima.

A.2.1.3. Resultats

Els resultats pel càlcul del mòdul resistent són els següents:

Element	**L_i (mm)**	**t_{eff} (mm)**	**A_i (mm^2)**	**σ_r (N/mm^2)**	**z (mm)**	**M (kN·mm)**
Corner 1inf	2,30	0,59	1,33	270,55	7,81	2818,65
1	10,50	0,59	6,16	270,55	4,00	7976,02
Corner 1sup	2,30	0,59	1,33	323,78	0,19	95,10
21	11,30	0,59	6,65	377,00	0,00	0,00
22	10,70	0,71	7,58	377,00	0,00	0,00
Corner 2sup	3,60	0,71	2,57	377,00	0,48	463,46
31	16,10	0,71	11,40	377,00	9,44	40599,78
32	16,10	0,71	11,40	377,00	47,22	202998,90
33	2,60	0,71	1,88	377,00	57,83	40934,87
Corner 2inf	3,60	0,71	2,57	377,00	58,52	56778,20
4	27,00	0,71	19,16	377,00	59,00	426210,31
TOTAL			72,00		252,50	**674,97**

Taula A.32. Resultats del moment.

	PLAIN
$M_{el,Rd,eff}$ (kN·m/m)	6,59
$W_{res,eff}$ (mm^3/m)	17467,02

Taula A.33. Resultats del mòdul resistent.

Els resultats iteratius pel càlcul del moment d'inèrcia resistent són els següents:

Element	**L_i (mm)**	**t_{eff} (mm)**	**A_i (mm^2)**	**z (mm)**	**S_i (mm^3)**	**z_0 (mm)**
Corner 1inf	2,30	0,59	1,33	51,19	68,28	-20,60
1	10,50	0,59	6,16	55,00	338,72	-20,83
Corner 1sup	2,30	0,59	1,33	58,81	78,44	-24,64
21	11,30	0,59	6,65	59,00	392,32	-28,45
22	10,70	0,71	7,58	59,00	447,00	-28,64
Corner 2sup	3,60	0,71	2,57	58,52	150,61	-28,64
3	62,90	0,71	44,63	29,50	1316,60	-28,16
Corner 2inf	3,60	0,71	2,57	0,48	1,23	0,86
4	27,00	0,71	19,16	0,00	0,00	30,36
TOTAL			**92,00**		2793,02	**30,36**

Taula A.34. Resultats de la iteració 0 de l'eix neutre.

Element	**L_i (mm)**	**t_{eff} (mm)**	**A_i (mm^2)**	**z (mm)**	**S_i (mm^3)**	**z_0 (mm)**	**I_i (mm^4)**
Corner 1inf	2,30	0,59	1,33	51,19	68,28	-20,60	697,06
1	10,50	0,59	6,16	55,00	338,72	-20,83	3759,90
Corner 1sup	2,30	0,59	1,33	58,81	78,44	-24,64	1300,66
21	11,30	0,59	6,65	59,00	392,32	-28,45	5452,99
22	10,70	0,71	7,58	59,00	447,00	-28,64	6213,08
Corner 2sup	3,60	0,71	2,57	58,52	150,61	-28,64	1274,40
3	62,90	0,71	44,63	29,50	1316,60	-28,16	11469,40
Corner 2inf	3,60	0,71	2,57	0,48	1,23	0,86	1435,58
4	27,00	0,71	19,16	0,00	0,00	30,36	17666,98
TOTAL			**92,00**		2793,02	**30,36**	**49270,06**

Taula A.35. Resultats de la iteració 1 de l'eix neutre.

	PLAIN
$I_{EN,eff}$ (mm^4/m)	480683,49

Taula A.36. Resultats del moment d'inèrcia resistent.

A.2.2. Moment negatiu

A.2.2.1. Ànima

Per calcular longitud no eficaç de l'ànima s_{Neff}, s'utilitzen les longituds equivalents $s_{eff,1}$ i $s_{eff,2}$:

$$s_{eff,0} = 0{,}95 \cdot t \cdot \sqrt{\frac{E}{\gamma_{M0} \cdot f_{yb}}} = 15{,}92\ mm$$

$$s_{eff,1} = s_{eff,0} = 15{,}92\ mm$$

$$s_{eff,n} = 1{,}5 \cdot s_{eff,0} = 23{,}88\ mm$$

	Iteració 0	Iteració 1	Iteració 2
s_{Neff} (mm)	-4,86 < 0	1,87	2,04

Taula A.37. Resultats iteratius de la longitud no eficaç de l'ànima.

A.2.2.2. Ala inferior

Mitjançant el procediment detallat en l'Eurocodi 3 es pot trobar l'esveltesa relativa pels diferents gruixos.

$$\overline{\lambda_p} = \sqrt{\frac{f_{yb}}{\sigma_{cr}}} = \frac{\frac{\bar{b}}{t}}{\left(28{,}4 \cdot \varepsilon \cdot k_\sigma^{\frac{1}{2}}\right)} = 1{,}80$$

$$\varepsilon = \sqrt{\frac{235}{f_{yb}}} = 0{,}79$$

El factor de vinclament utilitzat és $k_\sigma = 4$ i $\bar{b} = b_{p2}$.

Ja es pot calcular el factor reductor ρ que varia segons el material utilitzat. En el cas que ens pertoca, per l'acer, s'utilitzarà la següent formula:

$$\rho = \frac{1 - 0{,}55 \cdot \frac{(3+\psi)}{\overline{\lambda_p}}}{\overline{\lambda_p}} = 0{,}49$$

El rati de tensions (σ_2/σ_1) és $\psi = 1$.

Aquest factor en indica si cal considerar que la regió $\bar{b}$ en tota la seva longitud és o no efectiva. Per tant la longitud eficaç de la zona plana de l'ala és:

$$b_{eff} = \rho \cdot \bar{b} = 13{,}98\,mm$$

La longitud utilitzada és $\bar{b} = b_{p2}$

A.2.2.3. Resultats

Els resultats iteratius pel càlcul del moment d'inèrcia resistent i el mòdul resistent són els següents:

Element	**L_i (mm)**	**t_{eff} (mm)**	**A_i (mm^2)**	**z (mm)**	**S_i (mm^3)**	**z_0 (mm)**
Corner 1inf	2,30	0,71	1,61	7,81	12,55	12,65
1	10,50	0,71	7,42	4,00	29,69	16,47
Corner 1sup	2,30	0,71	1,61	0,19	0,30	20,28
2	28,80	0,71	20,46	0,00	0,00	20,47
Corner 2sup	3,60	0,71	2,57	0,48	1,23	19,99
3	62,90	0,71	44,63	29,50	1316,60	-9,03
Corner 2inf	3,60	0,71	2,57	58,52	150,61	-38,06
4	5,30	0,71	3,74	59,00	220,49	-38,53
TOTAL			**81,18**		1731,47	**20,47**

Taula A.38. Resultats de la iteració 0 de l'eix neutre.

Element	**L_i (mm)**	**t_{eff} (mm)**	**A_i (mm^2)**	**z (mm)**	**S_i (mm^3)**	**z_0 (mm)**
Corner 1inf	2,30	0,71	1,61	7,81	12,55	12,51
1	10,50	0,71	7,42	4,00	29,69	16,32
Corner 1sup	2,30	0,71	1,61	0,19	0,30	20,13
2	28,80	0,71	20,46	0,00	0,00	20,32
Corner 2sup	3,60	0,71	2,57	0,48	1,23	19,84
3	60,99	0,71	43,30	29,50	1277,35	-9,18
Corner 2inf	3,60	0,71	2,57	58,52	150,61	-38,20
4	5,30	0,71	3,74	59,00	220,49	-38,68
TOTAL			**83,28**		1692,2	**20,32**

Taula A.39. Resultats de la iteració 1 de l'eix neutre.

Element	**L_i (mm)**	**t_{eff} (mm)**	**A_i (mm^2)**	**z (mm)**	**S_i (mm^3)**	**z_0 (mm)**	**I_i (mm^4)**
Corner 1inf	2,30	0,71	1,61	7,81	12,55	12,50	251,01
1	10,50	0,71	7,42	4,00	29,69	16,31	2000,21
Corner 1sup	2,30	0,71	1,61	0,19	0,30	20,12	650,56
2	28,80	0,71	20,46	0,00	0,00	20,31	8437,04
Corner 2sup	3,60	0,71	2,57	0,48	1,23	19,83	632,03
3	60,82	0,71	43,18	29,50	1273,92	-9,19	14008,36
Corner 2inf	3,60	0,71	2,57	58,52	150,61	-38,21	2347,17
4	5,30	0,71	3,74	59,00	220,49	-38,69	5594,98
TOTAL			**83,16**		1688,79	**20,31**	**33921,35**

Taula A.40. Resultats de la iteració 2 de l'eix neutre.

	PLAIN
$I_{EN,eff}$ (mm^4/m)	330939,98
$W_{res,eff}$ (mm^3/m)	8553,14

Taula A.41. Resultats del moment d'inèrcia resistent.

A.3. Perfil EMB

A.3.1. Moment positiu

A.3.1.1. Ala superior

Mitjançant el procediment detallat en l'Eurocodi 3 es pot trobar l'esveltesa relativa pels diferents gruixos.

$$\overline{\lambda_p} = \sqrt{\frac{f_{yb}}{\sigma_{cr}}} = \frac{\frac{\bar{b}}{t}}{\left(28{,}4 \cdot \varepsilon \cdot k_\sigma^{\frac{1}{2}}\right)} = 0{,}99$$

$$\varepsilon = \sqrt{\frac{235}{f_{yb}}} = 0{,}79$$

El factor de vinclament utilitzat és $k_\sigma = 4$ i $\bar{b} = b_{p2}$.

Ja es pot calcular el factor reductor ρ que varia segons el material utilitzat. En el cas que ens pertoca, per l'acer, s'utilitzarà la següent formula:

$$\rho = \frac{1 - 0{,}55 \cdot \frac{(3+\psi)}{\overline{\lambda_p}}}{\overline{\lambda_p}} = 0{,}78$$

El rati de tensions (σ_2/σ_1) és $\psi=1$.

Aquest factor en indica si cal considerar que la regió $\bar{b}$ en tota la seva longitud és o no efectiva. Per tant la longitud eficaç de la zona plana de l'ala és:

$$b_{eff} = \rho \cdot \bar{b} = 24{,}80\,mm$$

La longitud utilitzada és $\bar{b} = b_{p2}$

S'obté l'àrea eficaç de la part dels rigiditzadors de l'ala superior. S'utilitza el procediment indicat en la normativa EN 1993-1-3:2006 [2]. Primer es calcula una secció eficaç (Taula A.42) utilitzant les especificacions de la Fig. A.10.

Fig. A.10. Figura 5.11 de EN 1993-1-3:2006 [2].

Element	L_i (mm)	A_i (mm^2)
Part plana (Fig. A.10)	11,29	8,01
Corner 1sup	2,26	1,61
1	10,45	7,42
Corner 1inf	2,26	1,61
Corner 1inf	2,26	1,61
1	10,45	7,42
Corner 1sup	2,26	1,61
Part plana (Fig. A.10)	11,29	8,01
TOTAL		**37,30**

Taula A.42. Primer càlcul de la secció eficaç de l'ala superior.

També s'obté una primera inèrcia eficaç (Taula A.43) segons la Fig. A.10.

Element	L_i (mm)	A_i (mm^2)	Z (mm)	S_i (mm^3)	z_0 (mm)	I_i (mm^4)
Part plana (Fig. A.10)	9,54	6,77	0,00	0,00	2,48	41,90
Corner 1sup	2,30	1,61	0,19	0,30	2,29	8,43
1	10,50	7,42	4,00	29,69	-1,52	43,73
Corner 1inf	2,30	1,61	8,19	13,16	-5,71	52,41
Corner 1inf	2,30	1,61	8,19	13,16	-5,71	52,41
1	10,5	7,42	4,00	29,69	-1,52	43,73
Corner 1sup	2,30	1,61	0,19	0,30	2,29	8,43
Part plana (Fig. A.10)	9,54	6,77	0,00	0,00	2,48	41,90
TOTAL		34,82		86,30	2,48	**292,94**

Taula A.43. Primer càlcul del moment inèrcia eficaç de l'ala superior.

Es calcula la tensió crítica:

$$\sigma_{cr,s} = \frac{4{,}2 \cdot k_w \cdot E}{A_s} \cdot \sqrt{\frac{I_s \cdot t^3}{4 \cdot {b_p}^2 \cdot (2 \cdot b_p + 3 \cdot b_s)}} = 480{,}90\ MPa$$

$$k_w = k_{w0} = 1{,}48$$

$$k_{w0} = \sqrt{\frac{s_w + 2 \cdot b_d}{s_w + 0{,}5 \cdot b_d}} = 1{,}48$$

$$l_b = 3{,}07 \cdot \sqrt[4]{\frac{I_s \cdot {b_p}^2 \cdot (2 \cdot b_p + 3 \cdot b_s)}{t^3}} = 317{,}37\ mm$$

L'alçada inclinada de l'ànima és $s_w = b_{p3}$. També s'utilitzen les longituds segons la Fig. A.11, el moment d'inèrcia i secció eficaç anteriors.

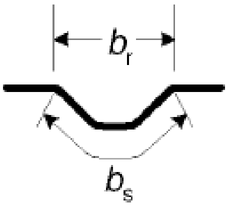

Fig. A.11. Figura 5.11 de EN 1993-1-3:2006 [2].

Es calcula el valor de l'esveltesa relativa i posteriorment un factor reductor:

$$\overline{\lambda_d} = \sqrt{\frac{f_{yb}}{\sigma_{cr,s}}} = 0{,}89$$

$$\chi_d = 1{,}47 - 0{,}723 \cdot \overline{\lambda_d} = 0{,}83$$

Finalment, el gruix reduït de la part de l'ala superior on està el rigiditzador i la part plana que té contacte directe segons la Fig. A.12.

$$t_{red} = \chi_d \cdot t = 0{,}59\,mm$$

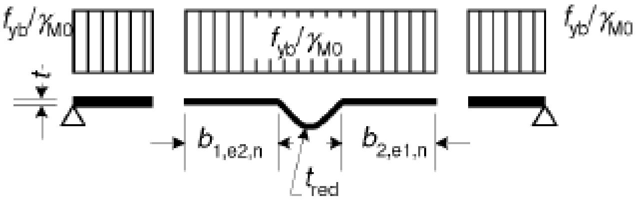

Fig. A.12. Figura 5.10 de EN 1993-1-3:2006 [2].

A.3.1.2. Ànima

Abans de la fallada de la secció es pot apreciar una petita plastificació parcial en la zona traccionada de l'ànima, mentre que la resta de la secció encara té un comportament elàstic.

En la primera aproximació de l'eix neutre s'assumeix que tota la l'ànima és completament efectiva i que la part del rigiditzador i la part plana de l'ala superior tenen la mateixa tensió com es mostra en la Fig. A.13.

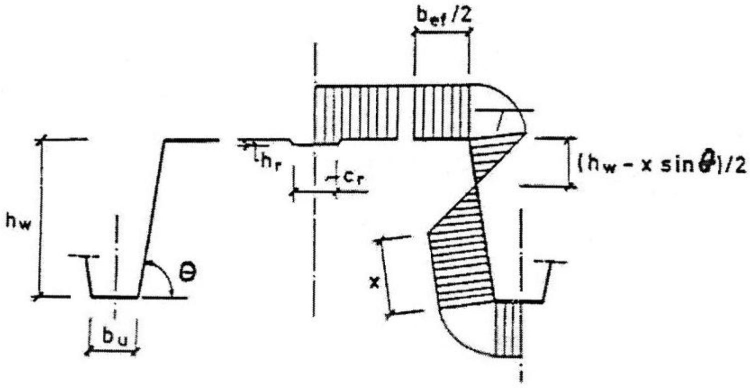

Fig. A.13. Primera aproximació de l'eix neutre efectiu.

Aplicant les condicions d’equilibri trobem, gràcies a un procés iteratiu, una primera aproximació de x i la tensió real (σr) que té el rigiditzador de l’ala superior (Taula A.30):

$$\frac{f_{yb}}{\gamma_{M0}} \cdot (A_{coner\,1inf} + A_1 + A_{corner\,1sup} + A_{21} + A_{22} + A_{corner\,2sup}) = \frac{f_{yb}}{\gamma_{M0}} \cdot (A_{coner\,2inf} + A_4)$$

$$\sigma_r = \frac{f_{yb}}{\gamma_{M0}} \cdot \left(1 - 2 \cdot \frac{h_r}{h - x \cdot \sin(\theta)}\right)$$

	Iteració 0	Iteració 1	Iteració 2	Iteració 3
x (mm)	5,48	2,59	2,65	2,64
σ_r (MPa)	266,64	270,65	270,55	270,55

Taula A.44. Resultats iteratius de la dimensió x.

Per calcular longitud no eficaç de l’ànima s_{Neff}, s’utilitzen les longituds equivalents $s_{eff,1}$ i $s_{eff,2}$. En quan a la longitud no eficaç de l’ànima s’ha de diferencia entre les usades en el càlcul del mòdul resistent i les usades en el càlcul del moment d’inèrcia.

$$s_{eff,0} = 0{,}95 \cdot t \cdot \sqrt{\frac{E}{\gamma_{M0} \cdot f_{yb}}} = 12{,}74\,mm$$

$$s_{eff,1} = s_{eff,0} = 12{,}74\,mm$$

$$s_{eff,n} = 1{,}5 \cdot s_{eff,0} = 19{,}10\,mm$$

<u>Mòdul resistent</u>

$$s_{Neff} = s_n - \left(s_{eff,1} + s_{eff,n}\right) = -3{,}50\,mm \geq 0$$

<u>Moment d’inèrcia</u>

	Iteració 0	Iteració 1	Iteració 2
s_{Neff} (mm)	-11,87 < 0	-9,35 < 0	-9,89 < 0

Taula A.45. Resultats iteratius de la longitud no eficaç de l’ànima.

Es calcula el gruix reduït necessari per tenir en compte les emboticions que existeixen en l’ànima segons:

$$t_{red,emb} = \rho \cdot t = 0{,}12\,mm$$

$$\rho = A \cdot h_{emb} + B = 0{,}17$$

El la constant A i B prenen els valor A = -0,112 i B = 0,368. La alçada de la embotició és de h_{emb} = 1,74 mm i la longitud de L_{emb} = 56,00 mm.

A.3.1.3. Resultats

Els resultats pel càlcul del mòdul resistent són els següents:

Element	**L_i (mm)**	**t_{eff} (mm)**	**A_i (mm^2)**	**σ_r (N/mm^2)**	**z (mm)**	**M (kN·mm)**
Corner 1inf	2,30	0,59	1,33	270,55	7,81	2818,65
1	10,50	0,59	6,16	270,55	4,00	7976,02
Corner 1sup	2,30	0,59	1,33	323,78	0,19	95,10
21	11,30	0,59	6,65	377,00	0,00	0,00
22	10,70	0,71	7,58	377,00	0,00	0,00
Corner 2sup	3,60	0,71	2,57	377,00	0,48	463,46
31	2,7	0,71	3,57	377,00	9,44	12716,44
31 (Emb.)	13,3	0,12				
32 (Emb.)	14,7	0,12	2,80	377,00	47,22	49763,19
32	1,4	0,71				
33	2,6	0,71	1,88	377,00	57,83	40934,87
Corner 2inf	3,60	0,71	2,57	377,00	58,52	56778,20
4	27,00	0,71	19,16	377,00	59,00	426210,31
TOTAL			55,61		252,50	**549,62**

Taula A.46. Resultats del moment.

	EMB
$M_{el,Rd,eff}$ (kN·m/m)	5,36
$W_{res,eff}$ (mm^3/m)	14223,12

Taula A.47. Resultats del mòdul resistent.

Els resultats iteratius pel càlcul del moment d'inèrcia resistent són els següents:

Element	L_i (mm)	t_{eff} (mm)	A_i (mm^2)	z (mm)	S_i (mm^3)	z_0 (mm)
Corner 1inf	2,30	0,59	1,33	51,19	68,28	-20,60
1	10,50	0,59	6,16	55,00	338,72	-20,83
Corner 1sup	2,30	0,59	1,33	58,81	78,44	-24,64
21	11,30	0,59	6,65	59,00	392,32	-28,45
22	10,70	0,71	7,58	59,00	447,00	-28,64
Corner 2sup	3,60	0,71	2,57	58,52	150,61	-28,64
3	62,90	0,71	44,63	29,50	1316,60	-28,16
Corner 2inf	3,60	0,71	2,57	0,48	1,23	0,86
4	27,00	0,71	19,16	0,00	0,00	30,36
TOTAL			**92,00**		2793,02	**30,36**

Taula A.48. Resultats de la iteració 0 de l'eix neutre.

Element	L_i (mm)	t_{eff} (mm)	A_i (mm^2)	z (mm)	S_i (mm^3)	z_0 (mm)
Corner 1inf	2,30	0,59	1,33	51,19	68,28	-20,34
1	10,50	0,59	6,16	55,00	338,72	-24,16
Corner 1sup	2,30	0,59	1,33	58,81	78,44	-27,97
21	11,30	0,59	6,65	59,00	392,32	-28,16
22	10,70	0,71	7,58	59,00	447,00	-28,16
Corner 2sup	3,60	0,71	2,57	58,52	150,61	-27,68
3	62,90	0,71	44,63	29,50	1316,60	1,34
Emb.	-56,00	0,71	-39,76	29,50	-1172,92	1,34
	56,00	0,12	6,88	29,50	203,06	1,34
Corner 2inf	3,60	0,71	2,57	0,48	1,23	30,37
4	27,00	0,71	19,16	0,00	0,00	30,84
TOTAL			**59,11**		1823,33	**30,84**

Taula A.49. Resultats de la iteració 1 de l'eix neutre.

Element	L_i (mm)	t_{eff} (mm)	A_i (mm^2)	z (mm)	S_i (mm^3)	z_0 (mm)	I_i (mm^4)
Corner 1inf	2,30	0,59	1,33	51,19	68,28	-20,34	665,27
1	10,50	0,59	6,16	55,00	338,72	-24,16	3615,55
Corner 1sup	2,30	0,59	1,33	58,81	78,44	-27,97	1257,10
21	11,30	0,59	6,65	59,00	392,32	-28,16	5271,57
22	10,70	0,71	7,58	59,00	447,00	-28,16	6006,37
Corner 2sup	3,60	0,71	2,57	58,52	150,61	-27,68	1231,29
3	62,90	0,71	44,63	29,50	1316,60	1,34	11516,74
Emb.	-56,00	0,71	-39,76	29,50	-1172,92	1,34	-8157,64
	56,00	0,12	6,88	29,50	203,06	1,34	1412,19
Corner 2inf	3,60	0,71	2,57	0,48	1,23	30,37	1482,10
4	27,00	0,71	19,16	0,00	0,00	30,84	18230,42
TOTAL			**59,11**		1823,33	**30,84**	**42530,96**

Taula A.50. Resultats de la iteració 2 de l'eix neutre.

	EMB
$I_{EN,eff}$ (mm^4/m)	414936,22

Taula A.51. Resultats del moment d'inèrcia resistent.

A.3.2. Moment negatiu

A.3.2.1. Ànima

Per calcular longitud no eficaç de l'ànima s_{Neff}, s'utilitzen les longituds equivalents $s_{eff,1}$ i $s_{eff,2}$:

$$s_{eff,0} = 0,95 \cdot t \cdot \sqrt{\frac{E}{\gamma_{M0} \cdot f_{yb}}} = 15,92\,mm$$

$$s_{eff,1} = s_{eff,0} = 15,92\,mm$$

$$s_{eff,n} = 1,5 \cdot s_{eff,0} = 23,88\,mm$$

	Iteració 0	Iteració 1	Iteració 2	Iteració 3	Iteració 4	Iteració 5
s_{Neff} (mm)	-4,86 < 0	1,87	8,83	10,69	11,27	11,45

Taula A.52. Resultats iteratius de la longitud no eficaç de l'ànima.

A.3.2.2. Ala inferior

Mitjançant el procediment detallat en l'Eurocodi 3 es pot trobar l'esveltesa relativa pels diferents gruixos.

$$\overline{\lambda_p} = \sqrt{\frac{f_{yb}}{\sigma_{cr}}} = \frac{\frac{\bar{b}}{t}}{\left(28{,}4 \cdot \varepsilon \cdot k_{\sigma}^{\frac{1}{2}}\right)} = 1{,}80$$

$$\varepsilon = \sqrt{\frac{235}{f_{yb}}} = 0{,}79$$

El factor de vinclament utilitzat és $k_\sigma = 4$ i $\bar{b} = b_{p2}$.

Ja es pot calcular el factor reductor ρ que varia segons el material utilitzat. En el cas que ens pertoca, per l'acer, s'utilitzarà la següent formula:

$$\rho = \frac{1 - 0{,}55 \cdot \frac{(3 + \psi)}{\overline{\lambda_p}}}{\overline{\lambda_p}} = 0{,}49$$

El rati de tensions (σ_2/σ_1) és $\psi=1$.

Aquest factor en indica si cal considerar que la regió $\bar{b}$ en tota la seva longitud és o no efectiva. Per tant la longitud eficaç de la zona plana de l'ala és:

$$b_{eff} = \rho \cdot \bar{b} = 13{,}98\, mm$$

La longitud utilitzada és $\bar{b} = b_{p2}$

A.3.2.3. Resultats

Els resultats iteratius pel càlcul del moment d'inèrcia resistent i el mòdul resistent són els següents:

Element	**L_i (mm)**	**t_{eff} (mm)**	**A_i (mm^2)**	**z (mm)**	**S_i (mm^3)**	**z_0 (mm)**
Corner 1inf	2,30	0,71	1,61	7,81	12,55	12,65
1	10,50	0,71	7,42	4,00	29,69	16,47
Corner 1sup	2,30	0,71	1,61	0,19	0,30	20,28
2	28,80	0,71	20,46	0,00	0,00	20,47
Corner 2sup	3,60	0,71	2,57	0,48	1,23	19,99
3	62,90	0,71	44,63	29,50	1316,60	-9,03
Corner 2inf	3,60	0,71	2,57	58,52	150,61	-38,06
4	5,30	0,71	3,74	59,00	220,49	-38,53
TOTAL			**81,18**		1731,47	**20,47**

Taula A.53. Resultats de la iteració 0 de l'eix neutre.

Element	**L_i (mm)**	**t_{eff} (mm)**	**A_i (mm^2)**	**z (mm)**	**S_i (mm^3)**	**z_0 (mm)**
Corner 1inf	2,30	0,71	1,61	7,81	12,55	6,52
1	10,50	0,71	7,42	4,00	29,69	10,33
Corner 1sup	2,30	0,71	1,61	0,19	0,30	14,14
2	28,80	0,71	20,46	0,00	0,00	14,33
Corner 2sup	3,60	0,71	2,57	0,48	1,23	13,85
3	60,99	0,71	43,30	29,50	1277,35	-15,17
Emb.	-56,00	0,71	-39,76	29,50	-1172,92	-15,17
	56,00	0,12	6,88	29,50	203,06	-15,17
Corner 2inf	3,60	0,71	2,57	58,52	150,61	-44,19
4	27,00	0,71	19,16	59,00	220,49	-44,67
TOTAL			**50,40**		722,35	**14,33**

Taula A.54. Resultats de la iteració 1 de l'eix neutre.

Element	**L_i (mm)**	**t_{eff} (mm)**	**A_i (mm^2)**	**z (mm)**	**S_i (mm^3)**	**z_0 (mm)**
Corner 1inf	2,30	0,71	1,61	7,81	12,55	4,88
1	10,50	0,71	7,42	4,00	29,69	8,69
Corner 1sup	2,30	0,71	1,61	0,19	0,30	12,50
2	28,80	0,71	20,46	0,00	0,00	12,69
Corner 2sup	3,60	0,71	2,57	0,48	1,23	12,21
3	54,03	0,71	38,36	29,50	1131,74	-16,81
Emb.	-56,00	0,71	-39,76	29,50	-1172,92	-16,81
	56,00	0,12	6,88	29,50	203,06	-16,81
Corner 2inf	3,60	0,71	2,57	58,52	150,61	-45,84
4	27,00	0,71	19,16	59,00	220,49	-46,31
TOTAL			**45,46**		576,74	**12,69**

Taula A.55. Resultats de la iteració 2 de l'eix neutre.

Element	**L_i (mm)**	**t_{eff} (mm)**	**A_i (mm^2)**	**z (mm)**	**S_i (mm^3)**	**z_0 (mm)**
Corner 1inf	2,30	0,71	1,61	7,81	12,55	4,37
1	10,50	0,71	7,42	4,00	29,69	8,18
Corner 1sup	2,30	0,71	1,61	0,19	0,30	11,99
2	28,80	0,71	20,46	0,00	0,00	12,18
Corner 2sup	3,60	0,71	2,57	0,48	1,23	11,70
3	54,17	0,71	37,04	29,50	1092,64	-17,32
Emb.	-56,00	0,71	-39,76	29,50	-1172,92	-17,32
	56,00	0,12	6,88	29,50	203,06	-17,32
Corner 2inf	3,60	0,71	2,57	58,52	150,61	-46,34
4	27,00	0,71	19,16	59,00	220,49	-46,82
TOTAL			**44,14**		537,65	**12,18**

Taula A.56. Resultats de la iteració 3 de l'eix neutre.

Element	**L_i (mm)**	**t_{eff} (mm)**	**A_i (mm^2)**	**z (mm)**	**S_i (mm^3)**	**z_0 (mm)**
Corner 1inf	2,30	0,71	1,61	7,81	12,55	4,21
1	10,50	0,71	7,42	4,00	29,69	8,02
Corner 1sup	2,30	0,71	1,61	0,19	0,30	11,83
2	28,80	0,71	20,46	0,00	0,00	12,02
Corner 2sup	3,60	0,71	2,57	0,48	1,23	11,54
3	51,59	0,71	36,63	29,50	1080,65	-17,48
Emb.	-56,00	0,71	-39,76	29,50	-1172,92	-17,48
	56,00	0,12	6,88	29,50	203,06	-17,48
Corner 2inf	3,60	0,71	2,57	58,52	150,61	-46,50
4	27,00	0,71	19,16	59,00	220,49	-46,98
TOTAL			**43,73**		525,66	**12,02**

Taula A.57. Resultats de la iteració 4 de l'eix neutre.

Element	L_i (mm)	t_{eff} (mm)	A_i (mm^2)	z (mm)	S_i (mm^3)	z_0 (mm)	I_i (mm^4)
Corner 1inf	2,30	0,71	1,61	7,81	12,55	4,16	27,78
1	10,50	0,71	7,42	4,00	29,69	7,97	497,76
Corner 1sup	2,30	0,71	1,61	0,19	0,30	11,78	223,00
2	28,80	0,71	20,46	0,00	0,00	11,97	2930,94
Corner 2sup	3,60	0,71	2,57	0,48	1,23	11,49	212,21
3	51,41	0,71	36,50	29,50	1076,83	-17,53	17476,62
Emb.	-56,00	0,71	-39,76	29,50	-1172,92	-17,53	-20306,55
	56,00	0,12	6,88	29,50	203,06	-17,53	3515,41
Corner 2inf	3,60	0,71	2,57	58,52	150,61	-46,55	3483,40
4	27,00	0,71	19,16	59,00	220,49	-47,03	8266,66
TOTAL			**43,60**		521,84	**11,97**	**16327,22**

Taula A.58. Resultats de la iteració 5 de l'eix neutre.

	EMB
$I_{EN,eff}$ (mm^4/m)	159289,97
$W_{res,eff}$ (mm^3/m)	3386,86

Taula A.59. Resultats del moment d'inèrcia resistent.

B. RESULTATS DELS ELEMENTS FINITS

B.1. Perfil KORONA 60

B.1.1. Modes de vinclament

A continuació es detallen els resultats obtinguts per a l’anàlisi per elements finits dels modes de vinclament.

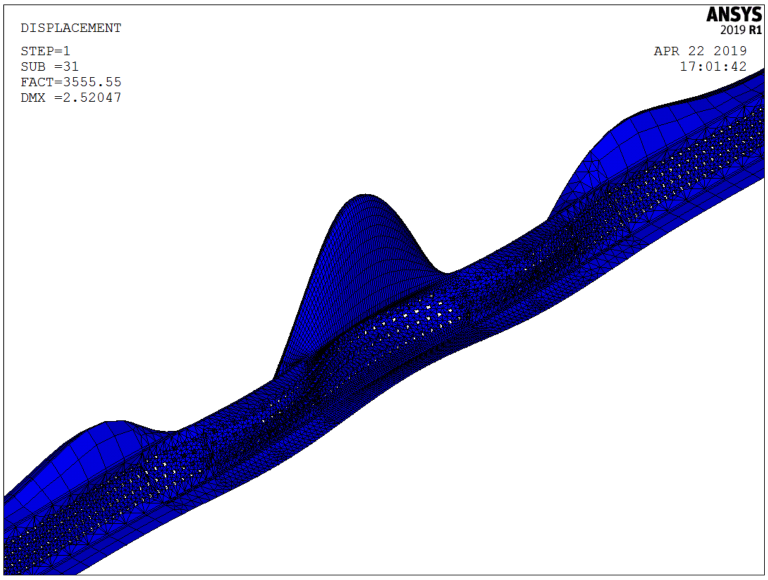

Fig. B.1. Mode de vinclament usat per crear la imperfecció inicial. t = 0,75 mm.

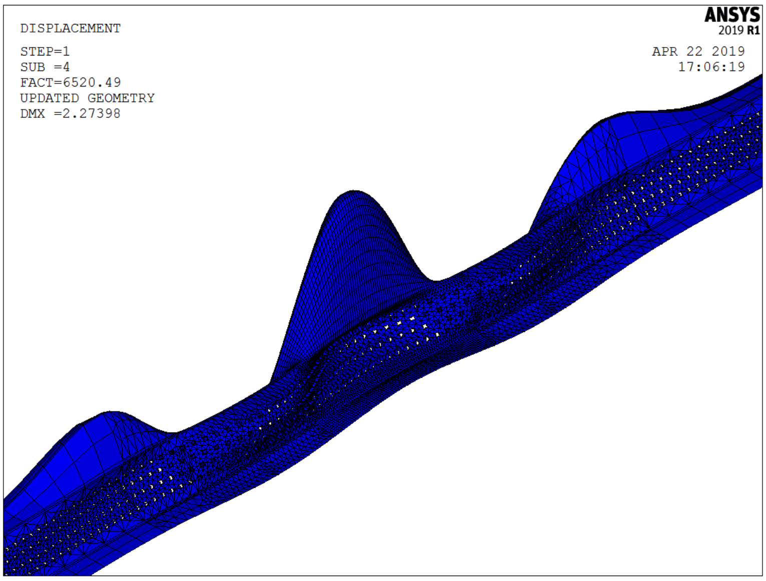

Fig. B.2. Mode de vinclament usat per crear la imperfecció inicial. t = 1,00 mm.

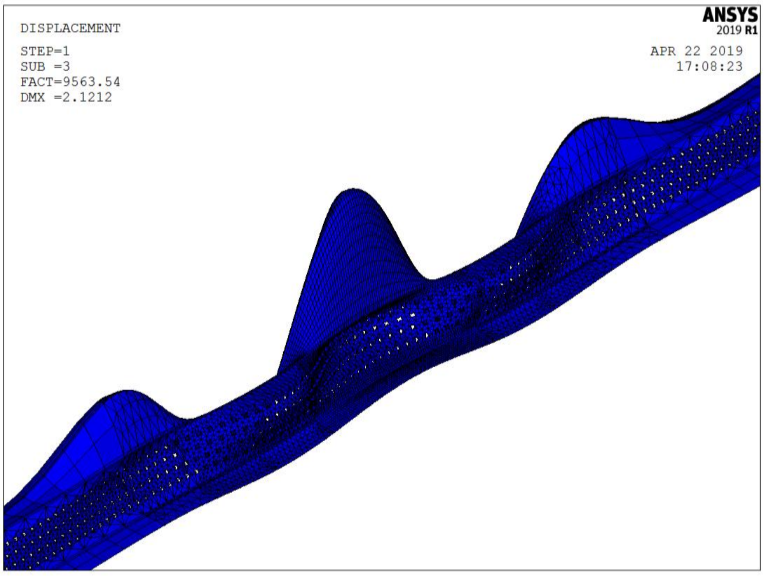

Fig. B.3. Mode de vinclament usat per crear la imperfecció inicial. t = 1,20 mm.

B.1.2. Estudi no lineal

A continuació es detallen els resultats obtinguts per a l'anàlisi no lineal per elements finits.

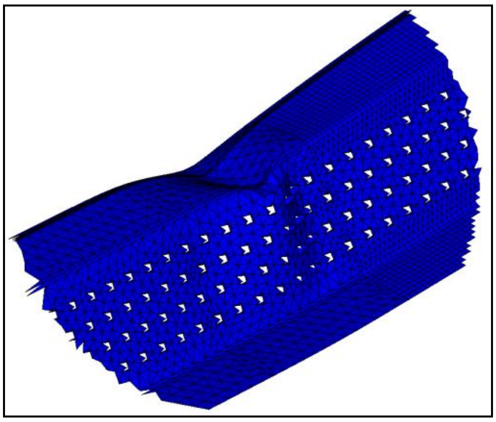

Fig. B.4. Formació de la ròtula.

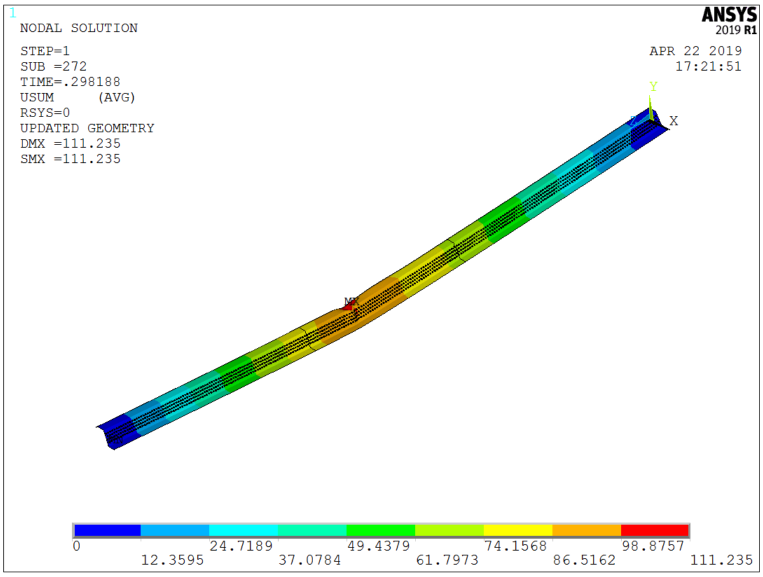

Fig. B.5. Diagrama de desplaçaments. t = 0,75 mm.

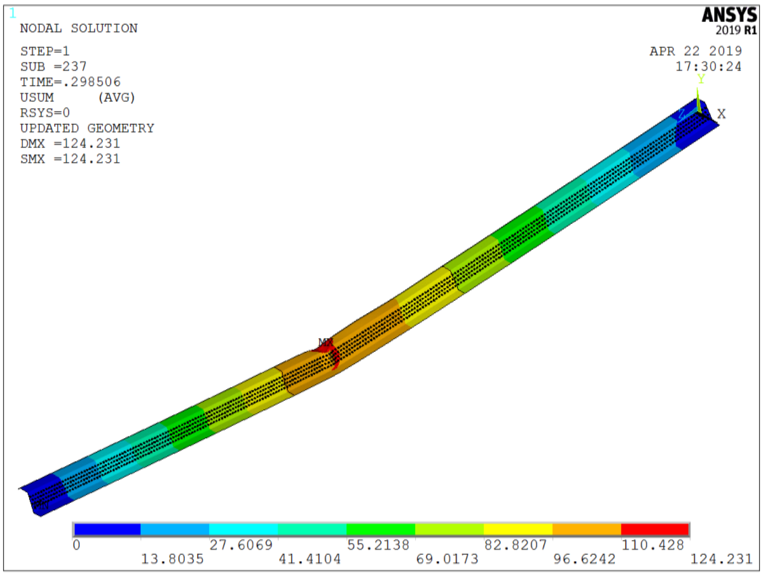

NODAL SOLUTION
STEP=1
SUB =237
TIME=.298506
USUM (AVG)
RSYS=0
UPDATED GEOMETRY
DMX =124.231
SMX =124.231

Fig. B.6. Diagrama de desplaçaments. t = 1,00 mm.

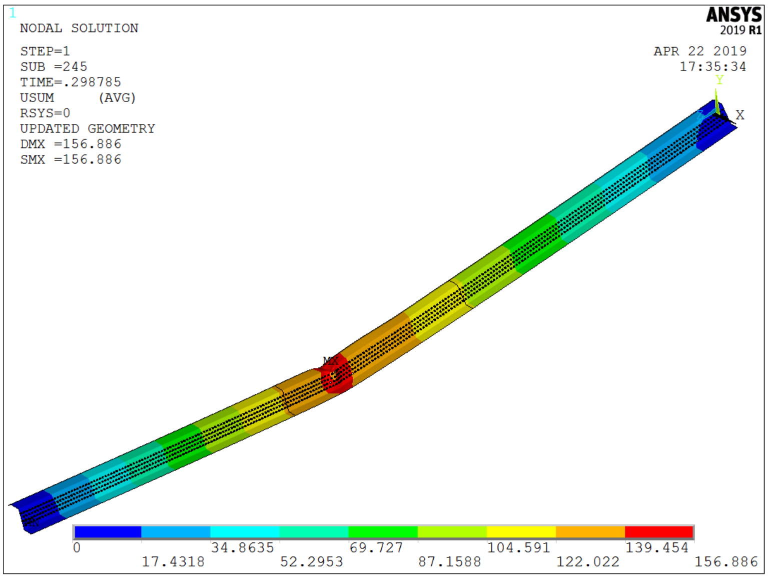

NODAL SOLUTION
STEP=1
SUB =245
TIME=.298785
USUM (AVG)
RSYS=0
UPDATED GEOMETRY
DMX =156.886
SMX =156.886

Fig. B.7. Diagrama de desplaçaments. t = 1,20 mm.

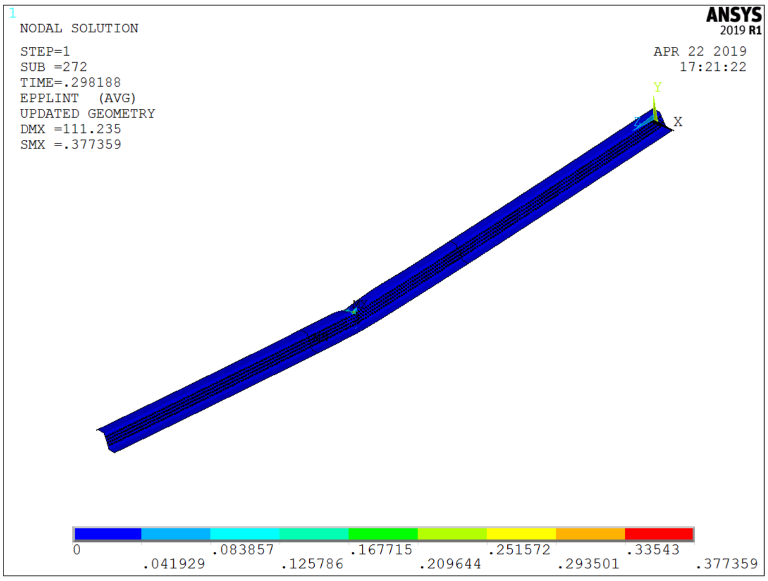

Fig. B.8. Diagrama del percentatge de plastificació. t = 0,75 mm.

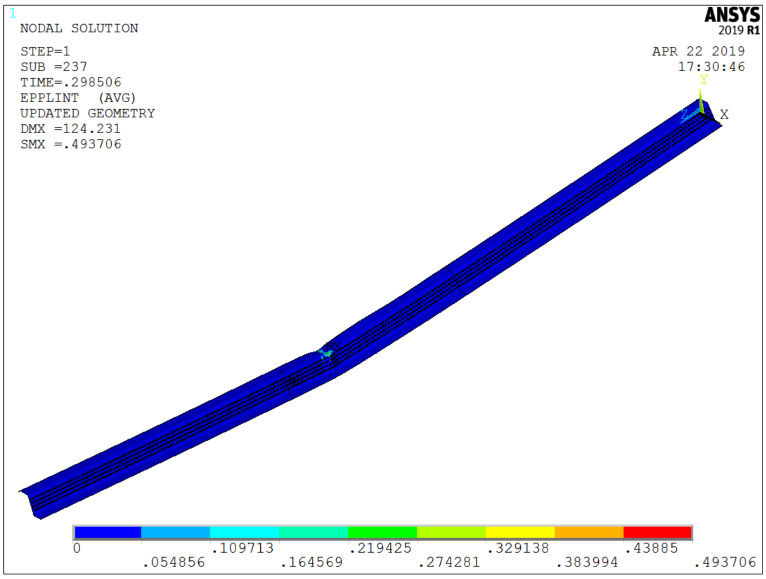

Fig. B.9. Diagrama del percentatge de plastificació. t = 1,00 mm.

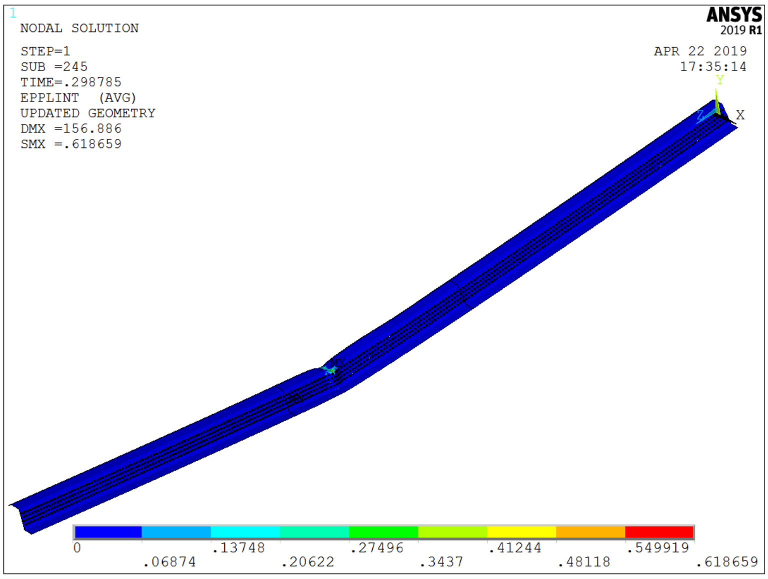

Fig. B.10. Diagrama del percentatge de plastificació. t = 1,20 mm.

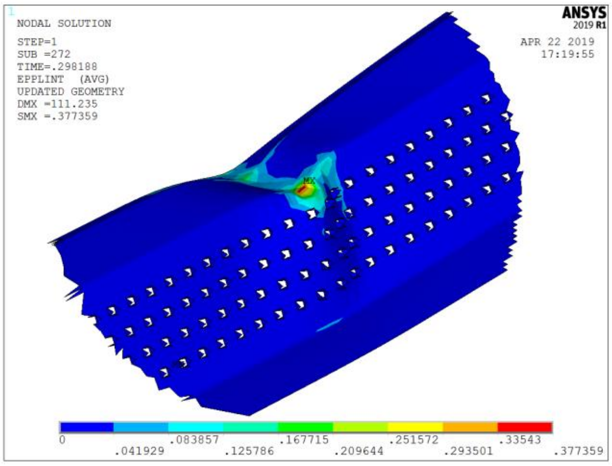

Fig. B.11. Detall del diagrama del percentatge de plastificació en la ròtula. t = 0,75 mm.

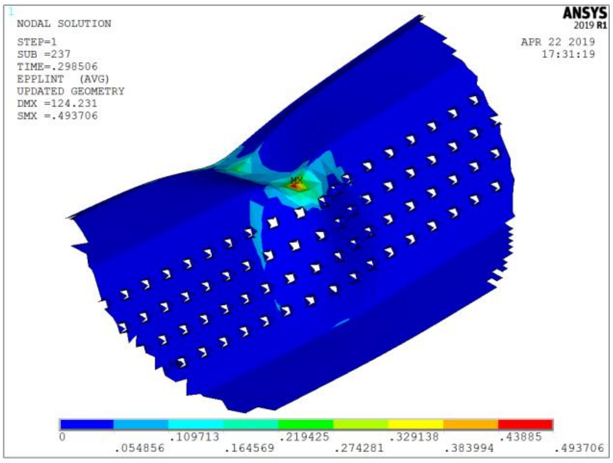

Fig. B.12. Detall del diagrama del percentatge de plastificació en la ròtula.
t = 1,00 mm.

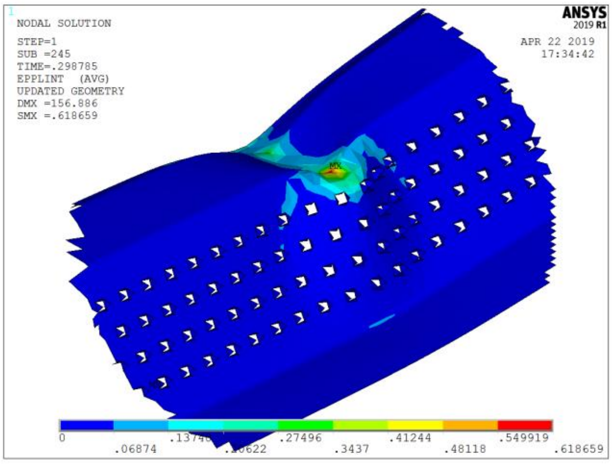

Fig. B.13. Detall del diagrama del percentatge de plastificació en la ròtula.
t = 1,20 mm.

B.2. Perfil PLAIN

B.2.1. Modes de vinclament

A continuació es detallen els resultats obtinguts per a l'anàlisi per elements finits dels modes de vinclament.

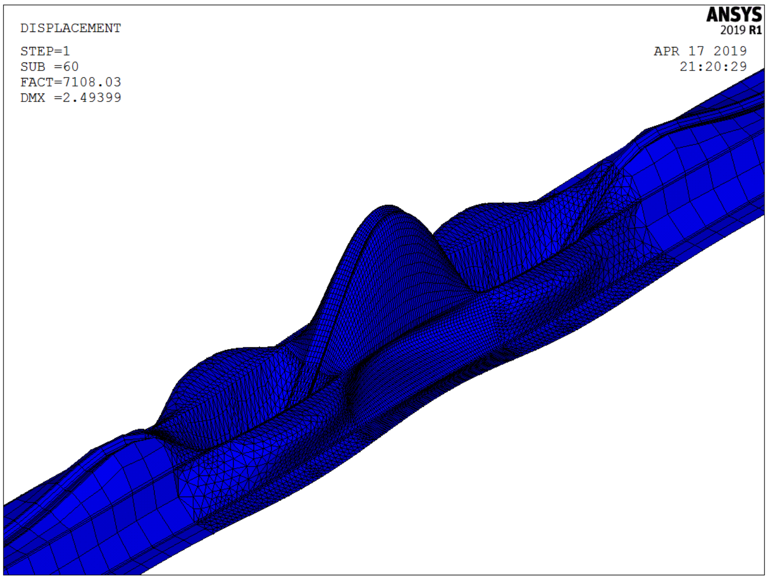

Fig. B.14. Mode de vinclament usat per crear la imperfecció inicial.

B.2.2. Estudi no lineal

A continuació es detallen els resultats obtinguts per a l'anàlisi no lineal per elements finits.

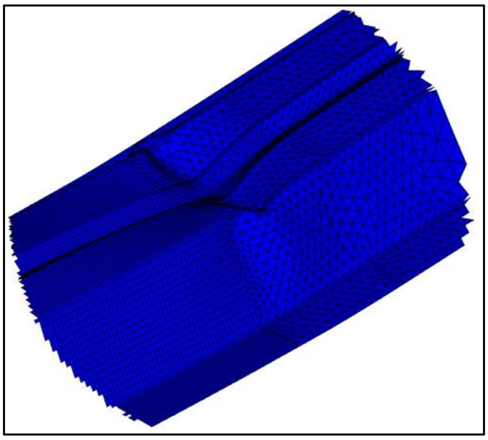

Fig. B.15. Formació de la ròtula.

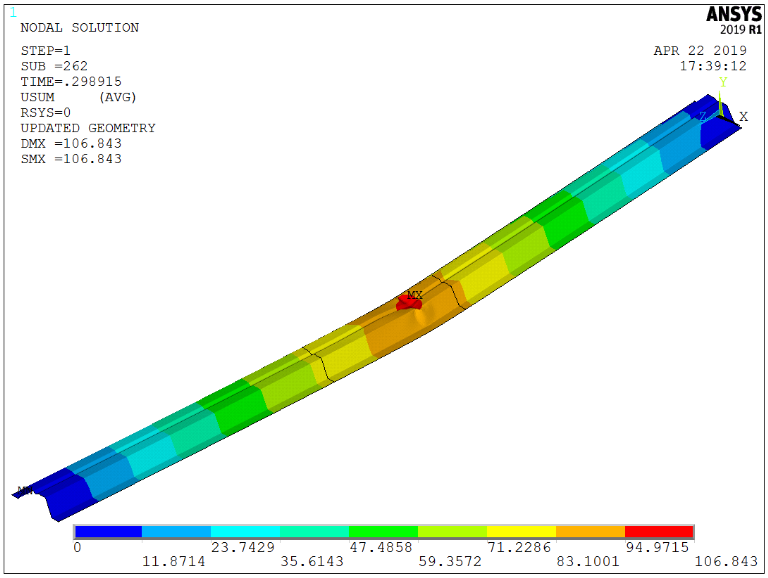

Fig. B.16. Diagrama de desplaçaments.

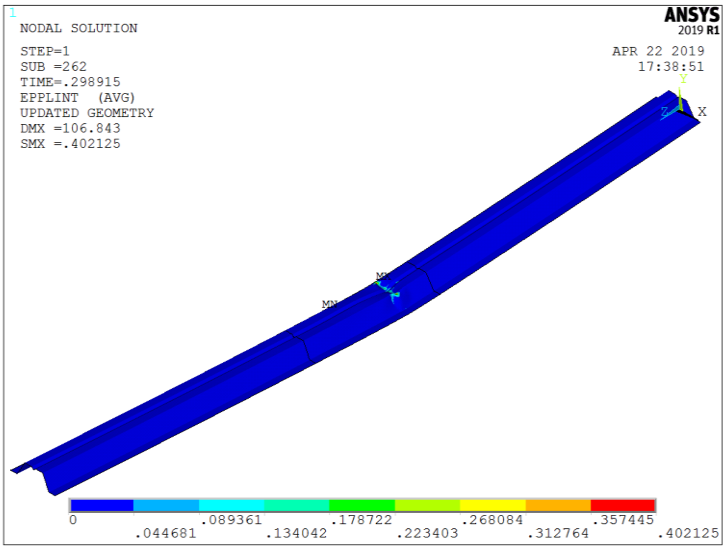

Fig. B.17. Diagrama del percentatge de plastificació.

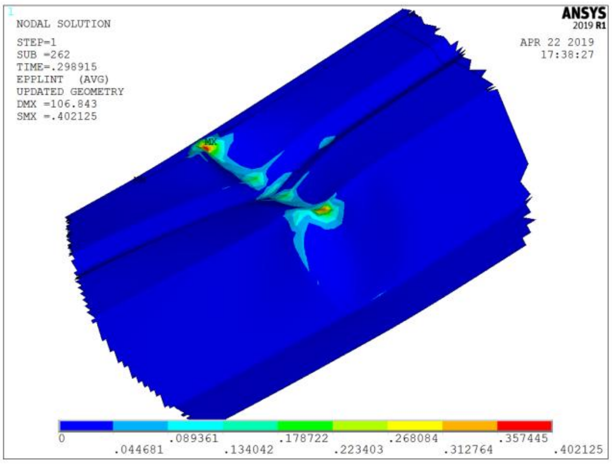

Fig. B.18. Detall del diagrama del percentatge de plastificació en la ròtula.

B.3. Perfil EMB

B.3.1. Modes de vinclament

A continuació es detallen els resultats obtinguts per a l'anàlisi per elements finits dels modes de vinclament.

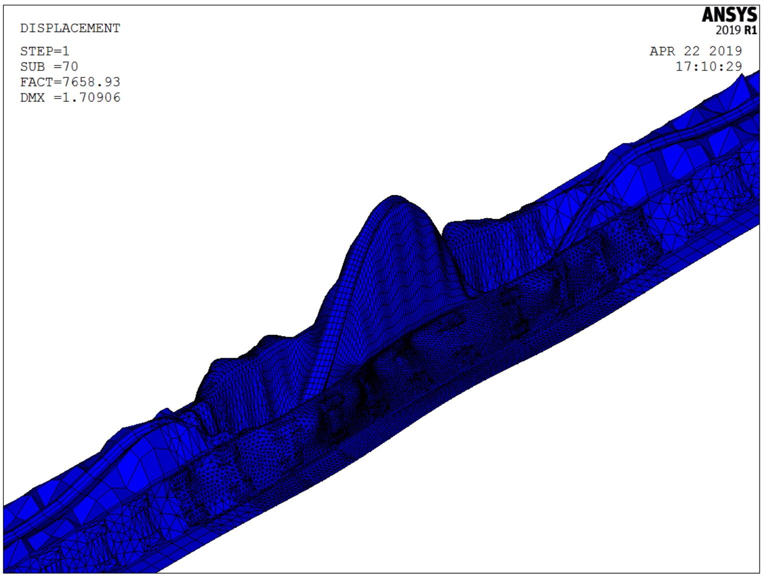

Fig. B.19. Mode de vinclament usat per crear la imperfecció inicial.

B.3.2. Estudi no lineal

A continuació es detallen els resultats obtinguts per a l’anàlisi no lineal per elements finits.

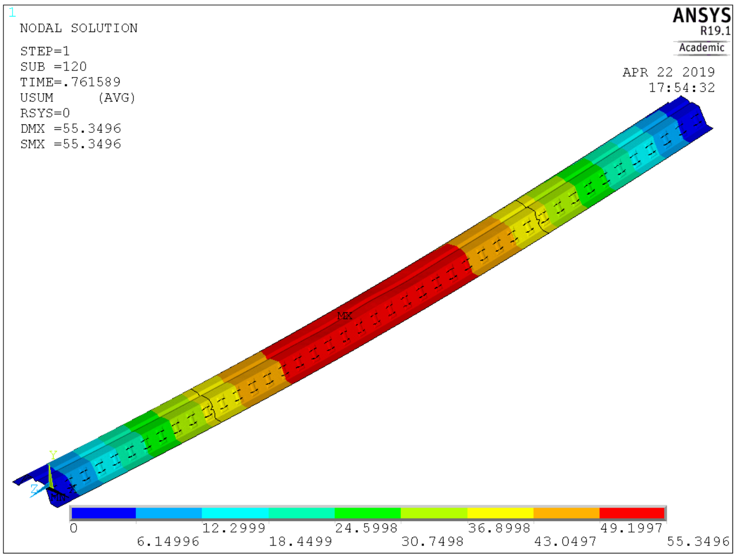

Fig. B.20. Diagrama de desplaçaments.

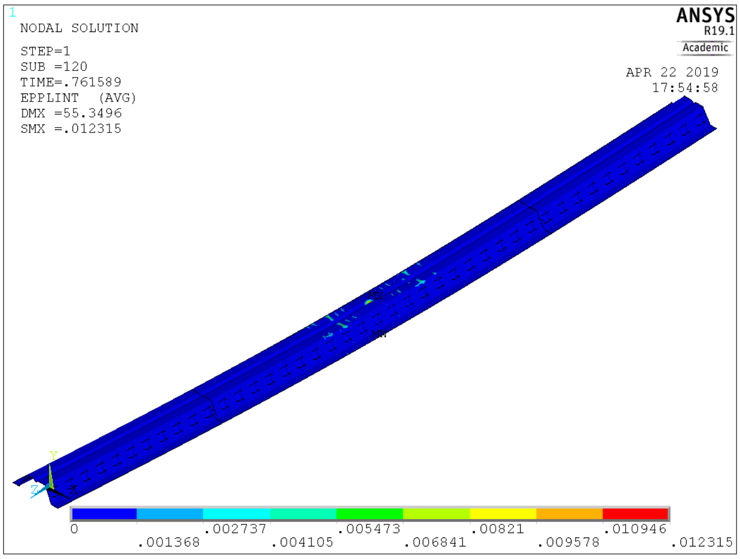

Fig. B.21. Diagrama del percentatge de plastificació.

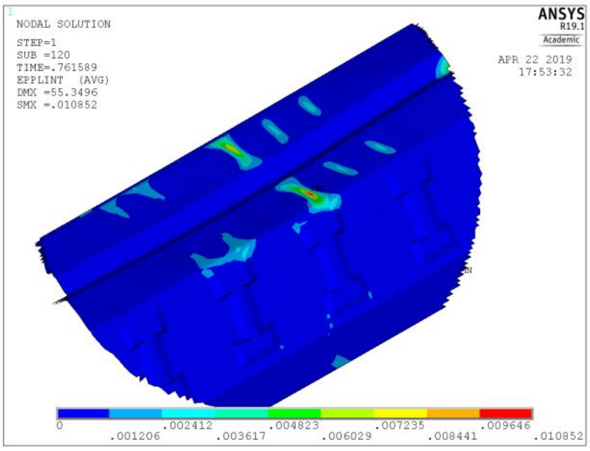

Fig. B.22. Detall del diagrama del percentatge de plastificació en la ròtula.

C. ARTICLE CIENTÍFIC

AN EXPERIMENTAL INVESTIGATION OF A NEW PERFECT BOND TECHNOLOGY FOR COMPOSITE SLABS. PART II: CONSTRUCTION STAGE

Frederic Marimon[*], Miquel Ferrer, Miquel Casafont, Carla Ripoll

Dept. of Strength of Materials and Structural Engineering
***Universitat Politècnica de Catalunya** · Barcelona**Tech (UPC)**, Spain*

Abstract

This article is the second part of a series related to an innovative full-connection bonding technology between steel sheet and concrete. The new UPC-system consists of producing bands of many small crown-shaped cuts in the sheeting webs, by a punching procedure, as a replacement for the conventional embossments. The high efficiency of the UPC-system in composite stage has been already analysed and published in this journal. The construction stage behaviour of this new system is presented now and compared with the same sheeting profile including the two conventional alternatives: embossments and plain profile. The results of single span bending tests –positive and negative– as well as internal support tests, demonstrate that the effect of the punches on the sheeting strength in construction stage is not significant and, in most cases the behaviour is even better performed than the design with the conventional embossments or the plain design.

Keywords

Composite slabs. Full shear connection. Constructional stage. Steel-deck bending. Internal support test.

1 Introduction

Steel-concrete slabs were first used in 1938 in the United States, although cold-formed steel sheeting was only used as permanent formwork. During the 1960s, steel decks with embossments were introduced and widely developed, the sheeting becoming the actual tensile reinforcement of the slab. The structural efficiency of

---

[*] Corresponding author.

E-mail address: frederic.marimon@upc.edu

composite slabs greatly depends on their ability to transfer shear forces between steel profile and concrete. The main difficulty of steel deck designing lies in assuring the effective composite performance; i.e., to conceive systems which are highly resistant to relative slip and debonding. To date, the conventional embossment system has shown to be unable to overcome the longitudinal shear failure mode, despite all attempts to improve embossment efficiency.

This article is the second part of a series related to the innovative full-connection bonding technology [1], named UPC-System and applied to *W60-MD* profile, consisting of a band of many small crown-shaped cuttings in the profile webs, as a replacement for the common embossments' system (Fig. 1*a*). The performance of the UPC-System had been already analysed and published in this journal regarding the composite stage [2]. In this article, the performance in construction stage is presented, where the sheeting is bearing the fresh concrete dead-load. According to EN 1993-1-3 [3], the analysis is made through the standard single span bending tests, positive M+ and negative M-, as well as the simplified *internal support test* (ITS).

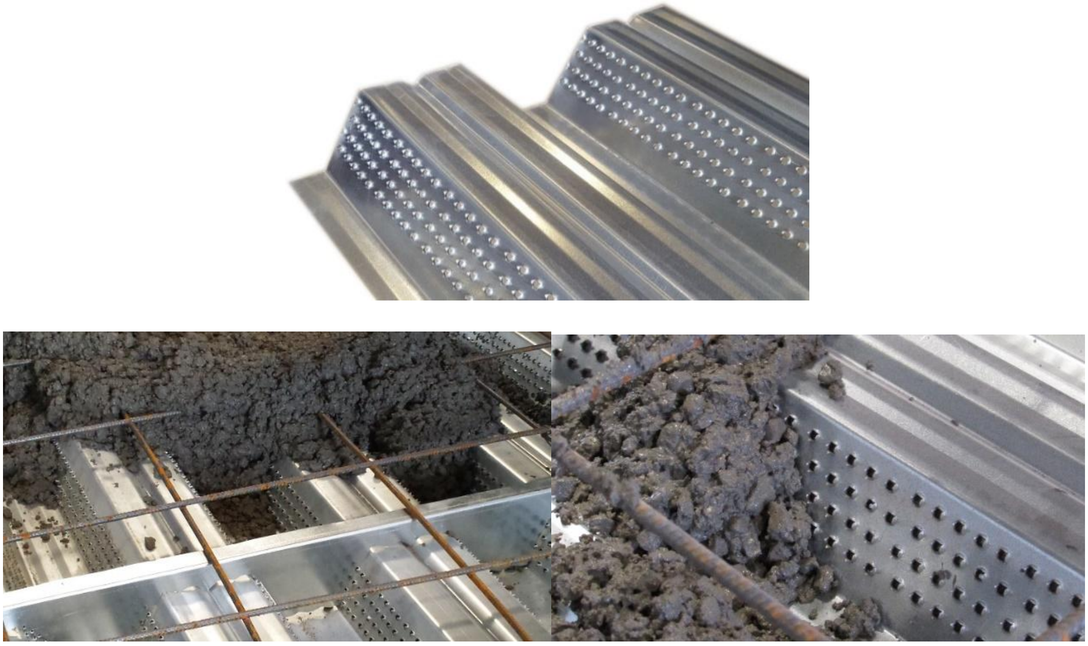

Fig. 1. W60-MD (UPC-system)

2 Characteristics of the elements

2.1. Profile dimensions

Three different sheeting designs have been studied, all of them based on the same commercial profile, named W60. The main design, named W60-MD from now on, corresponds to the new perfect bond UPC-system **¡Error! No se encuentra el origen de la referencia.**, and consists of a staggered punching on the webs (see Fig. 2a) with the *medium density* pattern [2]. In addition, two additional designs have been analysed in order to evaluate the differences on the response, using the very same profile, with respect to the conventional embossment system, named W60-Emb (**¡Error! No se encuentra el origen de la referencia.**b), and without neither perforations nor embossments but with flat surfaces, named W60-Plain (**¡Error! No se encuentra el origen de la referencia.**.b).

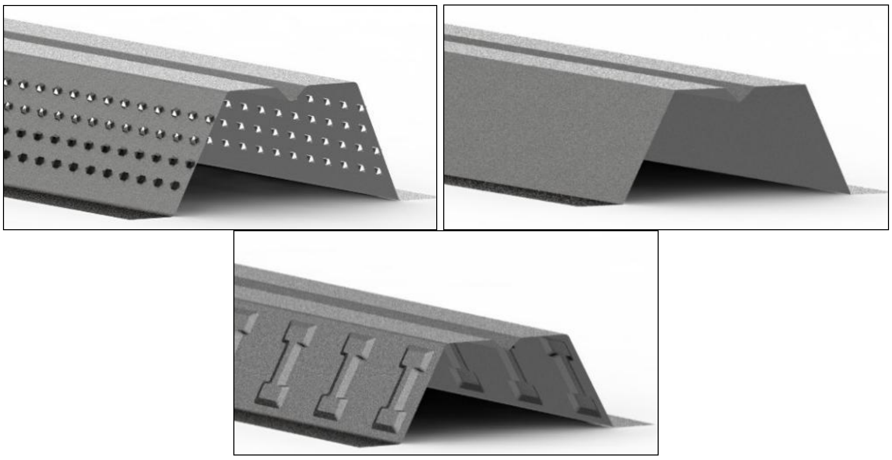

a) *b)*

c)

Fig. 2. Studied sheeting designs: a) W60-MD (UPC-system) b) W60-Plain c) W60-Emb.

Fig. 3 shows the general aspect of the W60-MD profile and its nominal dimensions. The studied sheeting is 59 mm high with a total width of 612 mm, corresponding to 3 profile ribs for positive bending test position (M$^+$, wide flange up), and 820 mm width for negative bending and internal support test positions (M$^-$, reversed, wide flange down), which corresponds to 4 ribs. The profile has been cut properly in order to avoid incomplete ribs or cantilever flanges. A detailed geometrical definition of the two flanges of a representative rib is shown in Fig. 4, including its longitudinal stiffeners. The two test types carried out in this work –single span bending test (M$^+$ and M$^-$) and internal support test (IST)– are described in Section 3.

Webs are inclined 62º including the punched pattern in order to guarantee a good connection to the concrete and to properly transfer the shear forces. This UPC-system consists of a regular staggered punching with 4 mm square punches on the lateral webs of the ribs, whose axes are separated 12 mm and 6 mm in transversal and longitudinal directions, respectively. The punching is produced on the sheeting so that the crown-shaped breakage is oriented towards the side of the sheeting to be in contact with the concrete.

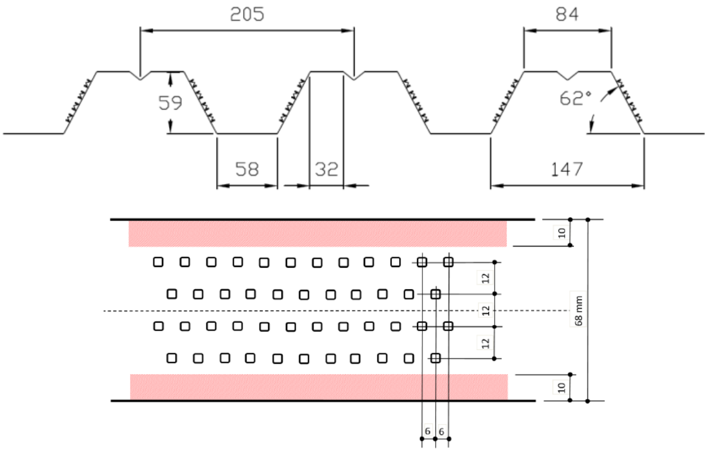

Fig. 3. W60-MD geometry.

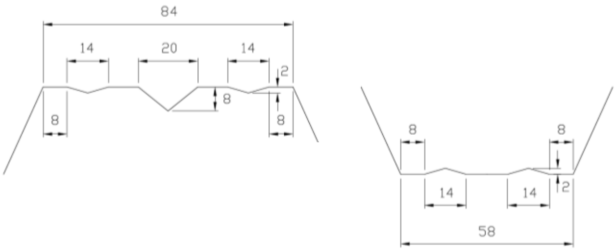

Fig. 4. Detailed geometry of a representative rib of the studied deck: wide flange (left) and narrow flange (right).

Several sheet thickness has been used for punched designs: 0.75, 1 and 1.2 mm for M^+, M^- bending tests; 0.75 and 1.2 mm for the IST with 1200, 700 and 400 mm in length. The additional tests with the embossed and the plain sheeting (see Fig. 5) are limited to a single thickness of 0.75 mm for single span bending test and, for the ITS, a thickness of 0.75 mm has been used for the W60-Plain design and the two thicknesses of 0.75 mm and 1.20 mm for the W60-Emb design.

The geometric characteristics and testing type of every specimen is shown in Table 1 and Table 2.

Table 1. Summary of specimens and test types.

Model	**Nominal thickness**	**Measured thickness**	**Net thickness**	**Test type**
	t_{nom} [mm]	t_{real} [mm]	t_{net} [mm]	Bending/IST span lengths
W60-MD – 0.75	0.75	0.75	0.71	M^+, M^- / IST 1200, 700, 400
W60-MD – 1.00	1.00	1.00	0.96	M^+, M^-
W60-MD – 1.20	1.20	1.20	1.16	M^+, M^- / IST 1200, 700, 400
W60-Plain – 0.75	0.75	0.75	0.71	M^+, M^- / IST 700
W60-Emb – 0.75	0.75	0.75	0.71	M^+, M^- / IST 1200, 700, 400
W60-Emb – 1.20	1.20	1.20	1.16	– / IST 1200, 700, 400

Table 2. Main dimensions.

Description		**Nominal value**	**Measured values**
		[mm]	[mm]
Profile high		59	58-60
Pitch length		205	205-206
Stiffener depths:	upper flange main	11	8
	upper flange lateral	2	1.0-1.5
	bottom flange	2	1.0-1.5

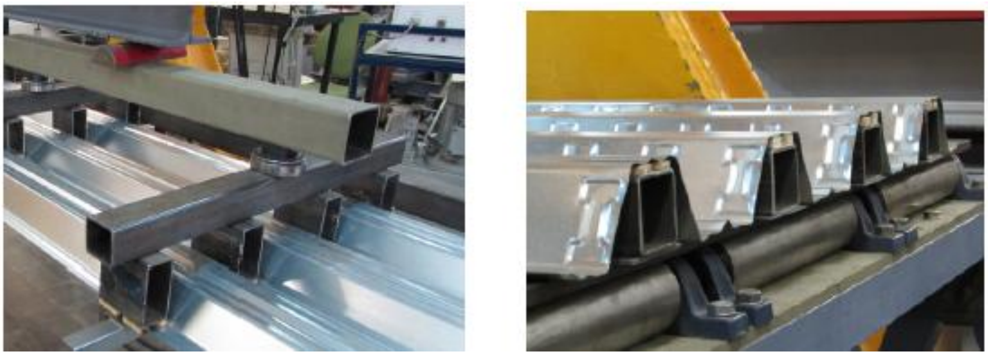

Fig. 5. Loading system detail with W60-Plain profile (left) and support detail with W60-Emb profile (right).

2.2. Steel properties

Each nominal thickness comes from different steel coils, but having a nominal quality corresponding to S320GD+Z275, according to EN 1993-1-3:2006 [3], with a nominal yield strength of f_y = 320 N/mm^2. This continuous sheet is galvanized on both sides with a zinc coating of 0.04 mm total thickness, equivalent of 275 g/m^2 mass. The yield strength, the breaking strength and the maximum elongation in % of the material of each coil have all been checked and summarised in Table 3.

Table 3. Properties of the steel tested.

Thickness *t* [mm]	**Steel**	$R_{p\,0.2\%}$ [N/mm^2]	R_m [N/mm^2]	***A80*** [%]
0.75	S320GD+Z	377	474	26
1.00	S320GD+Z	377	427	26.6
1.20	S320GD+Z	388	481	22

These results should be taken as a simple quality control since the cold forming process significantly alters them. The base material S320GD+Z reference values, before the cold-forming process, are the values used in the correction process described in Section 4.

3 Bending test setup and procedure

3.1. Single span bending test

According to Annex A (A.2.2) of EN 1993-1-3:2006 [3], the single span bending test is used to determine the pure bending resistance at the midspan, with no shear forces. Given that the cross-section is not symmetric, both positive (M^+) and negative (M^-) bending moment tests have been carried out. The span length is 3 m in all bending tests.

In order to ease the setup of a distributed loading (Fig. 6 left), Eurocode-3 presents a much simpler test layout having similar conditions (Fig. 6 right), with four transversal loads applied to the sheeting, placed at 375 mm from each support and equidistant from each other.

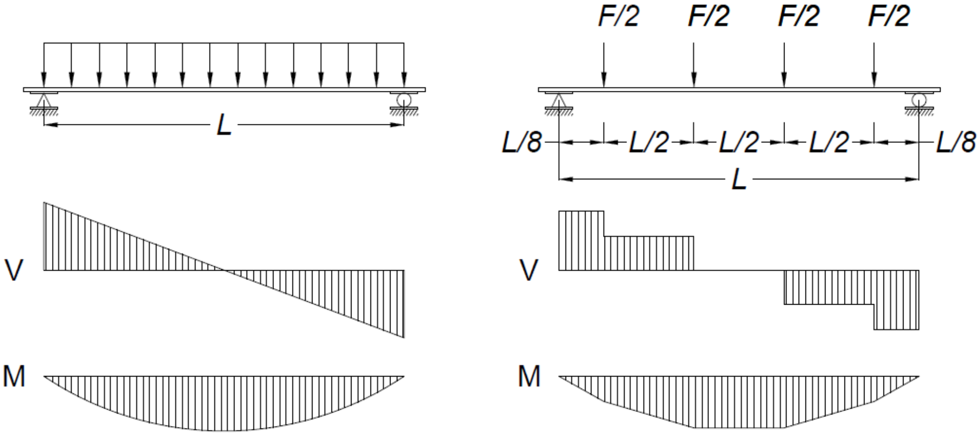

Fig. 6. Test setup for single span bending test and its respective shear and bending moment.

Three identical W60-MD specimens has been tested for each thickness (1.20, 1.00 and 0.75mm). The obtained results are shown in Section 5. Only one specimen has been tested of each additional design (W60-Plain and W60-Emb), having 0.75mm in thickness.

Regarding the setting up procedure, the sheeting is placed manually between the supports and screwed to the thick plate located on each support. In addition, according to Annex A (A.2.1) of EN 1993-1-3:2006 [3], an aluminium L angle is used to tie the lateral flanges right where the loads are applied in order to contribute to the lateral continuity of the sheeting in the real conditions.

As stated in Eurocode, hinged and roller supports has been be used to avoid any influence of rotational restraint at the supports on the results and to give the results a wide range of applicability.

Then, the system is centred and some rectangular steel tubes 100 mm long are placed at every loading line and at every rib. Two small 8 mm wood beams, bonded to the bottom side of the tubes, softly transfer the load to the sheeting (see Fig. 7), avoiding any rigid contact point or any damage on the lower flanges of the sheeting.

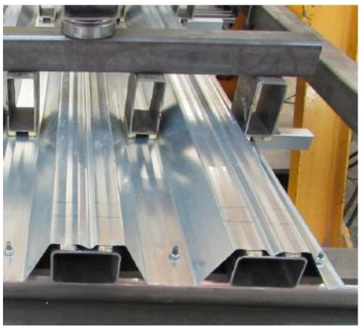

Fig. 7. Detail of the loading distribution system. Single span bending test.

The 60x60x4 mm transversal spreading beams are place over these small rectangular tubes and spherical bearings are used to transfer the load from the upper longitudinal spreading beams (100x100x4 mm) as shown in Fig. 8. An HE120B profile, which is initially suspended from the load cell, spreads the cylinder force on these longitudinal tubes by means of some half-round

supports.

The midspan deflection is measured by two resistive type displacement sensors d1-d2 located under the load (0.01mm resolution), 10 mm from the profile corners approximately. These sensors are set to zero after placing all of the load spreading elements but the main HE120B profile; therefore, the sheeting should be considered to be loaded by its weight and the self-weight of the load spreading elements.

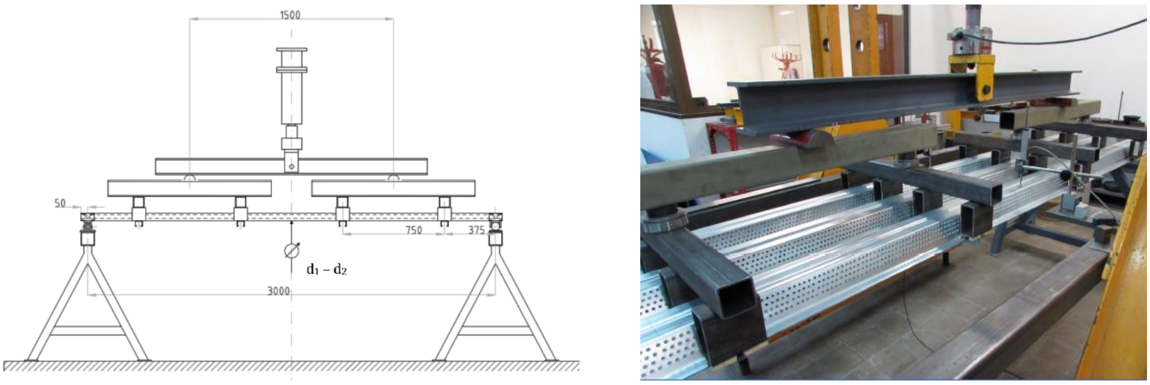

Fig. 8. Load spreading system in the single span bending test.

The applied force is measured thorugh a load cell with 50 kN force capacity, which is calibrated to zero while the central spreading beam is suspended. Consequently, the applied load is correctly measured by the load cell and includes the main beam weight:

$$F_{sensor} = Cylinder\ force + Central\ beam\ weight \qquad \textbf{(1)}$$

3.2. Double span test: Internal support test.

The double span test is a test set-up to determine the resistance of a continuous sheeting over two or more spans. The combination of bending moment and shear force is present at internal supports.

According to Annex A (A.2.3) of EN 1993-1-3:2006 [3], this combination should be analysed by a double-span bending test (see Fig. 9, left). However, the internal support test (ITS) is a much simpler test setup also included in Eurocode-3, though an equivalent bending moment and shear diagrams arrangement (see Fig. 9, right). In this reduced test, only one transversal force is applied at the midspan of a simply supported sheeting, having a span length equal to $s = 0.4\ L$.

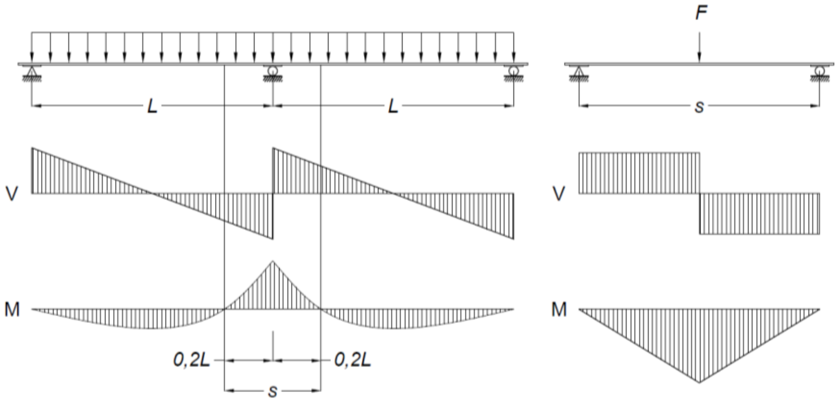

Fig. 9. Bending and shear diagram equivalence between double span (left) and internal support (right) tests.

Three span lengths have been analysed for W60-MD and W60-Emb designs: 1300 mm, 700 mm and 400 mm. Four specimens of each span length have been tested: two with 0.75 mm in thickness and two more with 1.2 mm. In the case of W60-Plain, only two specimens have been tested, having 700 mm span length and 0.75 mm sheet thickness.

The setting up procedure is similar to the single span bending test. The load was applied were an IPN60 spreading beam transversally placed at the midspan, and a 60 mm x 10 mm steel plate in between. A spherical bearing is placed below the cylinder for transferring the load (Fig. 10).

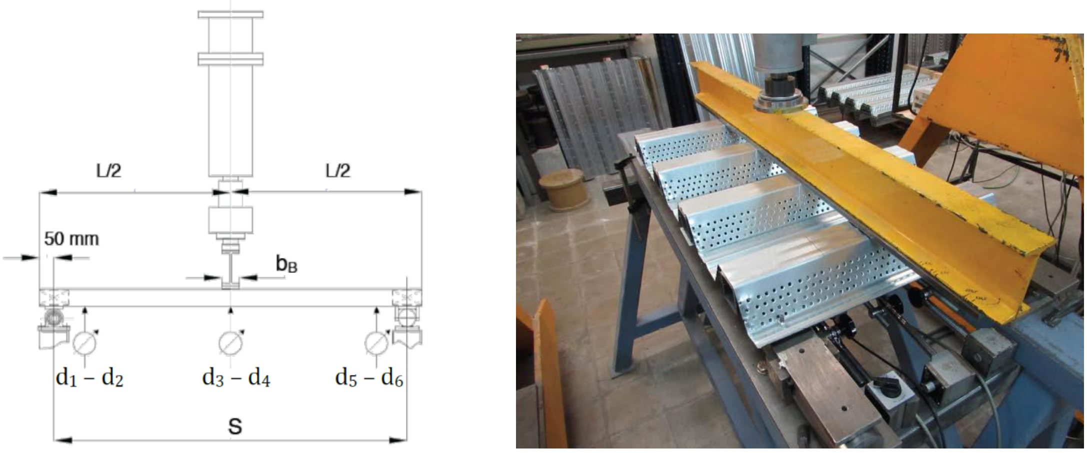

Fig. 10. Load spreading system. Internal support test.

The displacements were measured were six sensors, d1–d2 and d5–d6 were located near each support and d3–d4 at the midspan, under the load. All of them were pointing to the same cross-section points as for the single span bending test and were calibrated in the same way.

The applied load was measured using the same load cell but no spreading beam was suspended from in this case. So, the force measured by the load cell was directly the cylinder force.

$$F_{sensor} = Cylinder\ force \tag{2}$$

4 Correction of steel properties

The values obtained in the steel tensile tests must be corrected properly in order to take into account the statistical dispersion, the discrepancies in the nominal thickness and in the nominal yield strength f_{yb} = 320 N/mm^2 (reference value), and also the conversion of the tested plate width, b, to the standard width b = 1000 mm.

To obtain the characteristic value, f_k, according to Annex A of EN 1993-1-3:2006 [3], it is important to differentiate between the tests with three or more specimens and the ones with only one or two. Regarding the first one, the general procedure exposed in Annex D EN 1990-1-3:2002 [4] is followed, consisting of a normal distribution, in order to determine the characteristic strength. Thus, with N = 3, the factor k should be 3.37 which provides the desired characteristic value, according to Eq. (3).

$$f_k = f_m - k \cdot s \tag{3}$$

However, for a group of one or two tests, the statistic procedure is that for small number of tests exposed in Annex A (A.6.3.3) of EN 1993-1-3:2006 [3]. As corresponds to local buckling failure mode, the value η_k should be 0.85 (between 0.8 and 0.9). Therefore, the characteristic resistance R_k must be obtained using Eq. (4).

$$R_k = \eta_k \cdot R_m = 0.85\ R_m \tag{4}$$

In order to correct the width and the yield strength, the procedure described in the section A.6.2 (5), (6) and (7) of Annex A of EN 1993-1-3:2006 [1] is followed, where the coefficient μ_R is obtained through the Eq. (5).

$$\mu_R = \left(\frac{f_{yb,obs}}{f_{yb}}\right)^{\alpha} \left(\frac{t_{obs,cor}}{t_{cor}}\right)^{\beta} \quad \textbf{(5)}$$

where: $f_{yb,obs}$ corresponds to the tested yield strength for each thickness.

α depends on the case:

1.0 for M^+, as the plastic failure mode is considered by direct observation of the F-d curve (high ductility).

0.5 for M^-, as the local buckling failure mode is considered by direct observation of the F-d curve (low ductility).

$t_{obs,cor} = t_{cor}$ in all cases, so thickness correction is no necessary.

5. Test results and analysis Single span bending test

The total applied load consists of the cylinder force and the self-weight of the sheeting and spreading elements (Eq. (6).

$$F = [F_{sensor} + \text{Own sheet weight} + \text{Spreading beams}] \quad \textbf{(6)}$$

The self-weight is 0.63 kN for the positive bending (M^+) and 0.83 kN for negative bending (M^-).

5.1.1. Positive bending test

The initial formation of the first plastic hinge is observed in the centre of the section just before the collapse. Afterwards, the local buckling of the upper flange is developed, where the central stiffener subjected to compression initially collapses in the *distorsinal mode* [X] over the flange width (see Fig. 11). The results are shown in Fig. 12 and Table 4.

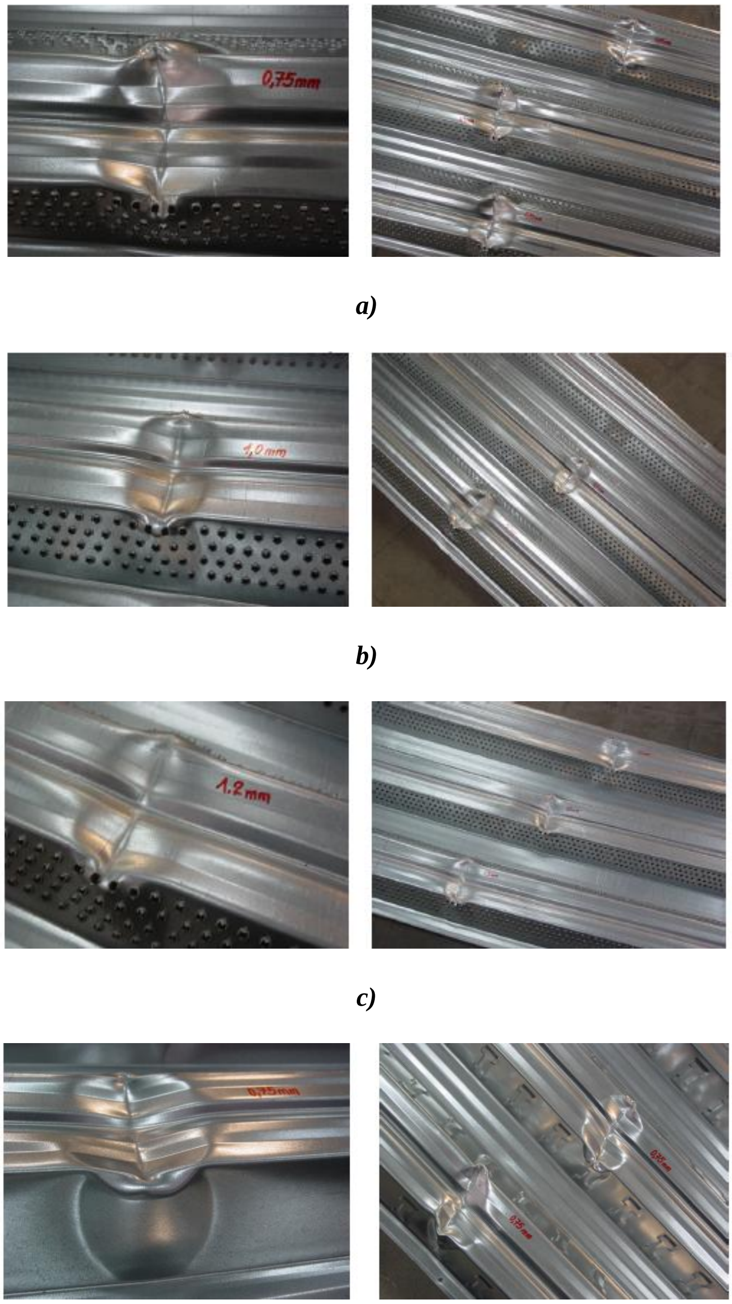

a)

b)

c)

d)

Fig. 11. Local buckling (M+): a) W60-MD–0.75 b) W60-MD 1.00 c) W60-MD–1.20 d) W60-Plain–0.75 and W60-Emb–0.75

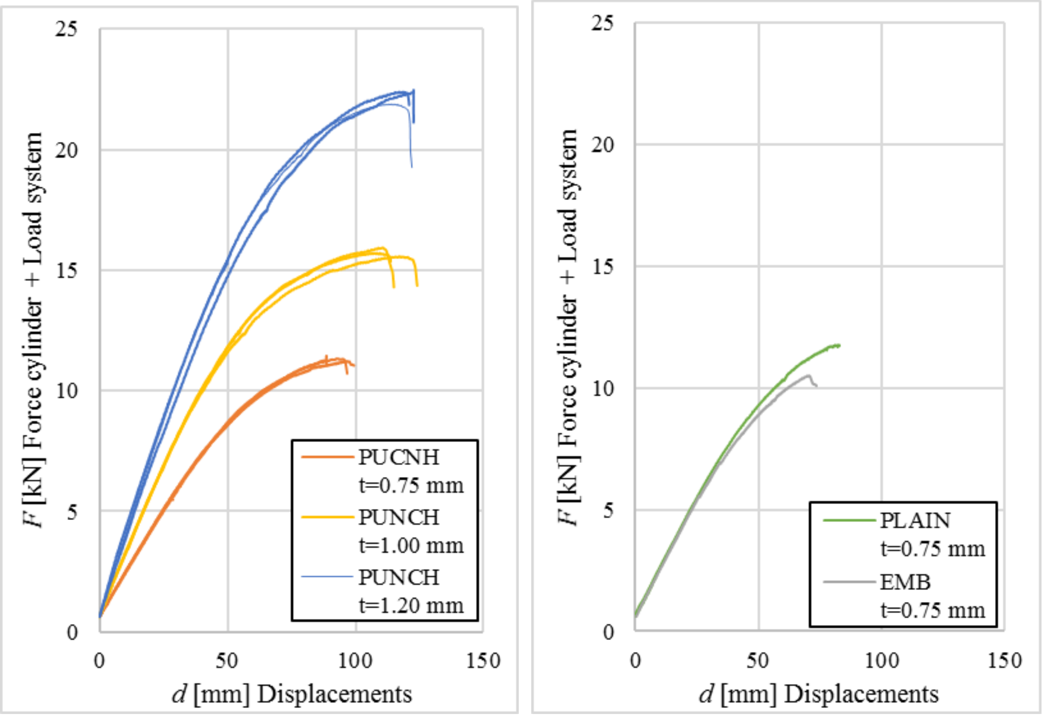

Fig. 12. F-d curves of the M^+ single span bending test.

Table 4. Results of the M^+ single span bending tests.

Model	$t_{nominal}$ [mm]	b [mm]	L [mm]	F_k [kN]	M_{Rk} [kNm/m]	W_{Rk} [mm^3/m]	I_{Rk} [mm^4/m]
W60-MD	0.75	615	3000	10.96	5.67	17.7	436.2
	1.00	615	3000	15.11	7.88	24.6	575.0
	1.20	615	3000	21.19	10.65	33.3	710.8
W60-Plain	0.75	615	3000	10.03	5.19	16.2	471.1
W60-Emb	0.75	615	3000	8.93	4.62	14.5	437.0

Eq. (7) and Eq. (8) are used to determine the characteristic bending moment and the characteristic section modulus.

$$M^{+}_{R,k} = \frac{1}{8} \cdot F_k \cdot L \qquad \textbf{(7)}$$

$$W^{+}_{Rk} = \frac{M^{+}_{Rk}}{f_{yb}} \tag{8}$$

The incremental values of the force and displacement are used in Eq. (9) to determine the moment of inertia. Thus, by simple observation of the graphs of the tests, the incremental values ΔF and $\Delta d = (\Delta d_1 + \Delta d_2)/2$ are chosen over a wide range of linear response (Fig. 13).

$$I^{+}_{R,k} = 0.0133073 \cdot \frac{\Delta F \cdot L^3}{E \cdot \Delta d} \tag{9}$$

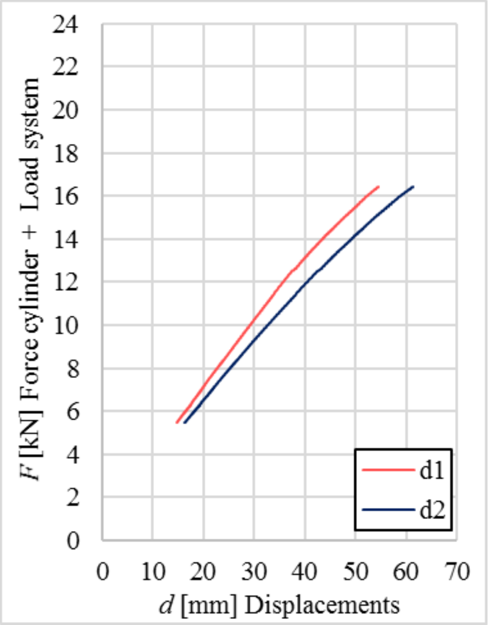

Fig. 13. Incremental values of force and displacement to calculate the moment of inertia.

5.1.2. Negative bending moment

The local buckling of the upper flange of the profile is observed just before the collapse, where the small longitudinal nerves do not prevent compression from causing the overall global buckling of the rib. Notice that the buckling direction (upwards or inwards) is random (see Fig. 14). The mechanism of collapse occurs indifferently according to the direct or inverse mode [X]. Results are shown in Table 5 and in Fig. 15.

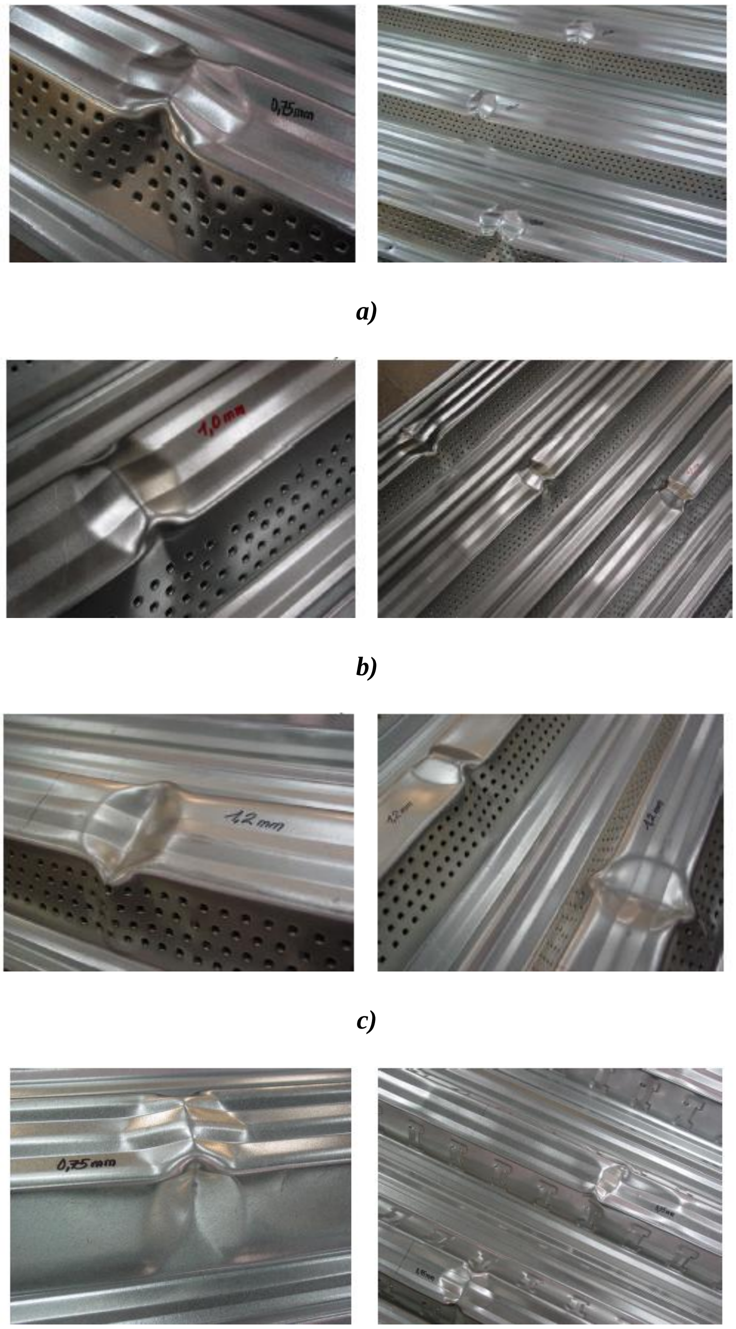

a)

b)

c)

d)

Fig. 14. M^{-} Test local buckling: a) W60-MD–0.75 b) W60-MD–1.00 c) W60-MD–1.20 d) W60-Plain–0.75 and W60-Emb–0.75

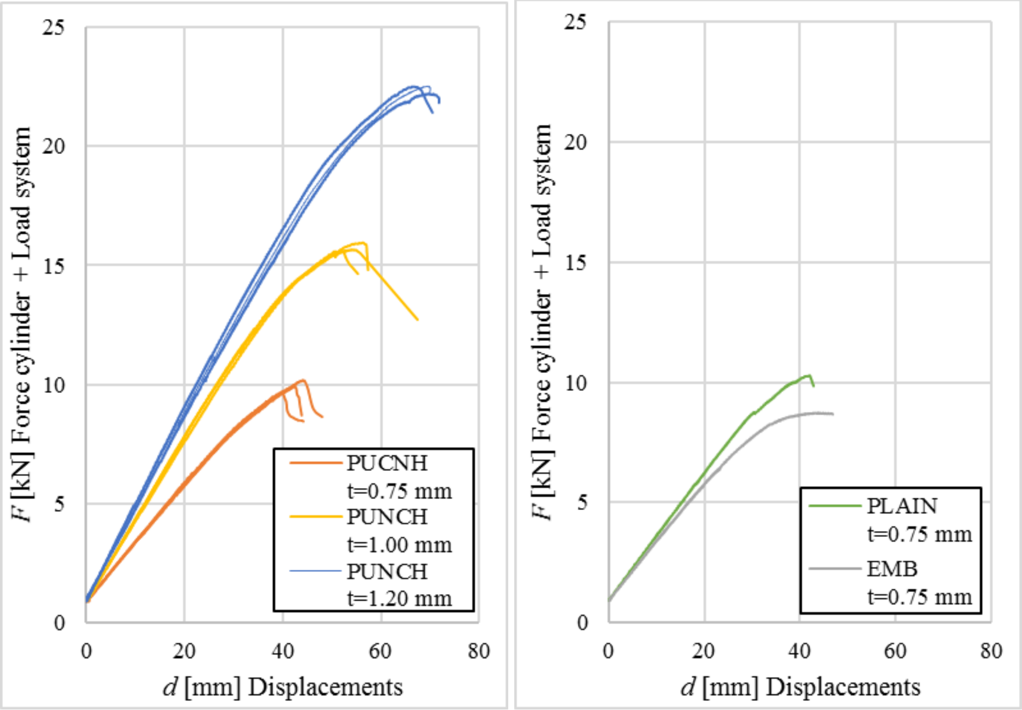

Fig. 15. F-d curves of the M^{-} single span bending test.

Table 5. Results of the M^{-} single span bending tests.

Model	$t_{nominal}$ [mm]	b [mm]	L [mm]	F_k [kN]	M_{Rk} [kNm/m]	W_{Rk} [mm^3/m]	I_{Rk} [mm^4/m]
W60-MD	0.75	820	3000	9.03	3.81	11.892	497.110
	1.00	820	3000	15.13	6.40	19.999	615.212
	1.20	820	3000	21.80	9.05	28.295	779.095
W60-Plain	0.75	820	3000	8.76	4.53	11.532	548.293
W60-Emb	0.75	820	3000	7.45	3.85	9.804	485.830

The same expressions than for the positive bending moment has been used to calculate these results.

The information extracted from the comparative graphs (Fig. 16) is the following:

i) The results for W60-Plain and W60-Emb are quite similar to those obtained for the W60-MD profile with the same thickness of 0.75 mm.

ii) In both tests, M^{+} and M^{-}, the final loads and stiffness are lightly higher in the case of the W60-Plain profile.

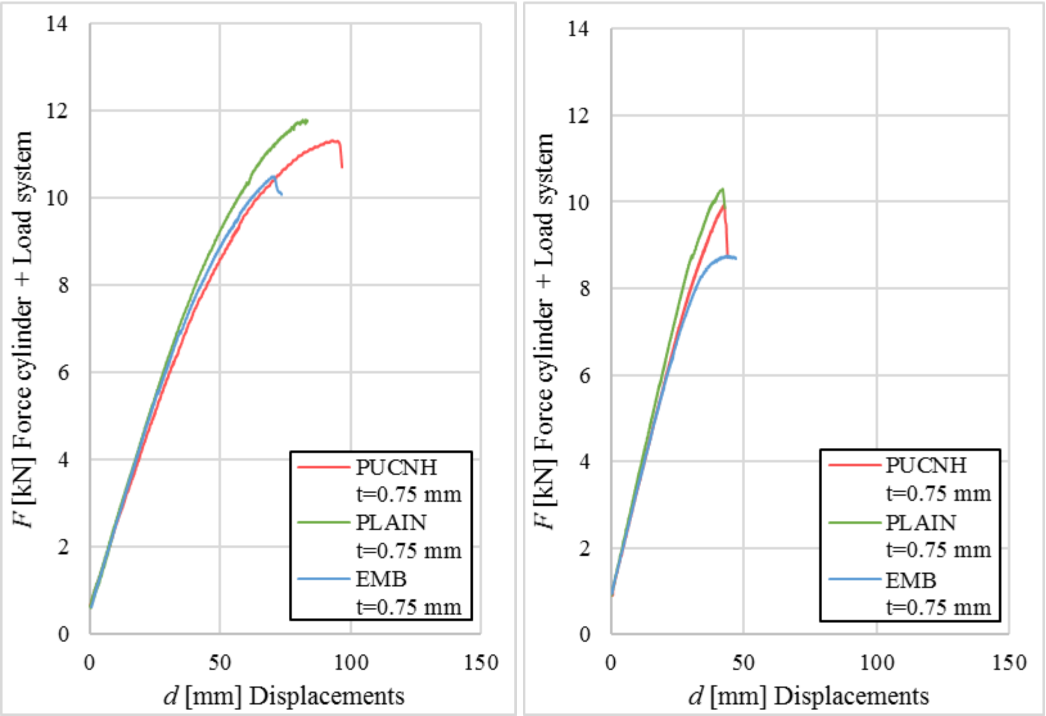

a) *b)*

Fig. 16. Comparative F-d curves for single span bending test: a) M$^+$ b) M$^-$.

5.2. Internal support test

The same method has been used to determinate the total load applied to the system, with an additional load of 0.20 kN.

Table 6. Results of the Internal support test.

Model	t_{nom}	b	L	F_k	M_{Ed}
	[mm]	[mm]	[mm]	[kN]	[kNm/m]
W60-MD	0.75	820	400	19.22	1.92
		820	700	14.04	2.52
		820	1200	10.07	3.27
	1.20	820	400	49.15	4.91
		820	700	36.86	6.45
		820	1200	23.24	7.55
W60-Plain	0.75	820	700	15.35	2.69

W60-Emb	0.75	820	400	21.37	2.14
		820	700	15.56	2.72
		820	1200	9.42	3.06
	1.20	820	400	48.69	4.87
		820	700	34.76	6.08
		820	1200	20.28	6.59

The characteristic bending moment at the support is determined through Eq. (10).

$$M_{Ed} = \frac{1}{4} \cdot F_u \cdot L \tag{10}$$

The failure mode is virtually identical, named *web crippling* [X]. Moderate variations on the ultimate loads are detected.

Internal support test results are summarized in Fig. 17. and the following three aspects are observed:

i) **Short spans**: for instance, L= 400/0.4 = 1000 mm

- for t = 0.75 mm: W60-MD provides 10% lower strength than W60-Emb.
- for t = 1.20 mm: W60-MD provides 2% higher strength than W60-Emb.

ii) **Medium spans**: for instance L= 700/0.4 = 1750 mm

- W60-MD gives similar strength than W60-Emb.
- W60-Plain specimens give intermediate values.

iii) **Large spans**: for instance L= 1.300/0.4 = 3250 mm

- for t = 0.75 mm W60-MD provides 11% higher strength than W60-Emb.
- for t = 1.2 mm W60-MD provides 13% higher strength than W60-Emb.

However, the dispersion of the experimental results cannot be conclusive about the exact differences between W60-MD design and W60-Emb. The early conclusion is that both systems do not show significant differences.

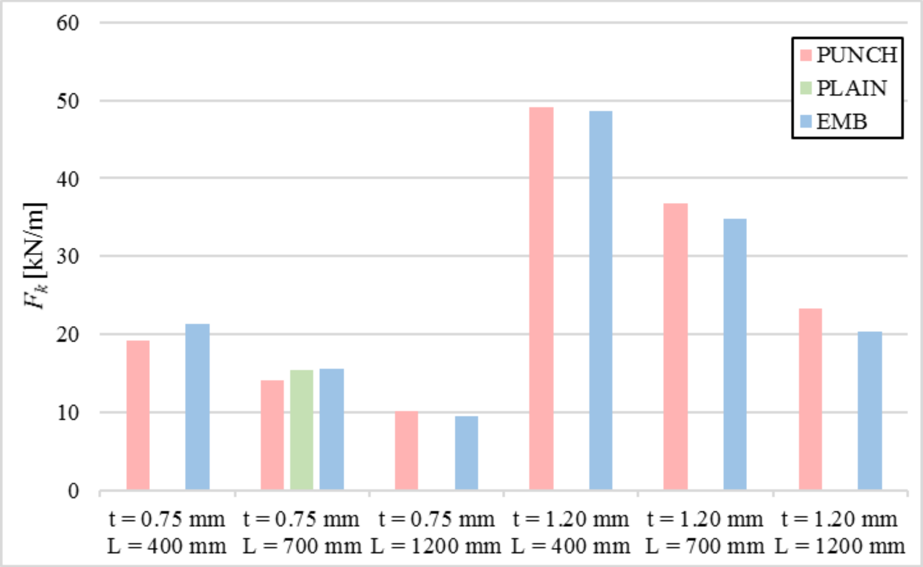

Fig. 17. Results comparison between W60-MD, W60-Emb and W60-Plain sheeting designs.

6. Moment-Reaction interaction diagram.

The M^{-}–R interaction diagram is calculated in order to compare the behaviour of each design and thickness.

The reaction $R_{W,Rd}$ was calculated through eq. (11) from EN 1993-1-3:2006, section 6.1.7.3 [1]

$$R_{w,Rd} = \alpha \cdot t^2 \cdot \sqrt{f_{yb} \cdot E} \cdot \left(1 - 0.1 \cdot \sqrt{\frac{r}{t}}\right) \cdot \left(0.5 + \sqrt{0.02 \cdot \frac{l_a}{t}}\right) \cdot \frac{2.4 + \left(\frac{\phi}{90}\right)^2}{\gamma_{M0}} \qquad \textbf{(11)}$$

On the other hand, the negative moment $M^{-}_{c.Rd}$ was directly obtained from the internal support tests (see 5.2).

The safety area in the M^{-}–R interaction diagram is limited by three segments: $M^{-}_{c.Rd}$ and $R_{W,Rd}$ limits corresponds to the horizontal and vertical limits, respectively; the third segment corresponds to eq. (12), where M_{Ed} and F_{Ed} parameters are free combinations of moment and reaction.

$$\frac{M_{Ed}}{M_{c,Rd}} + \frac{F_{Ed}}{R_{w,Rd}} \leq 1.25 \qquad \textbf{(12)}$$

Fig. 18 and Fig. 19 show the $M^{-}_{c.Rd} - R_{W,Rd}$ interaction diagrams.

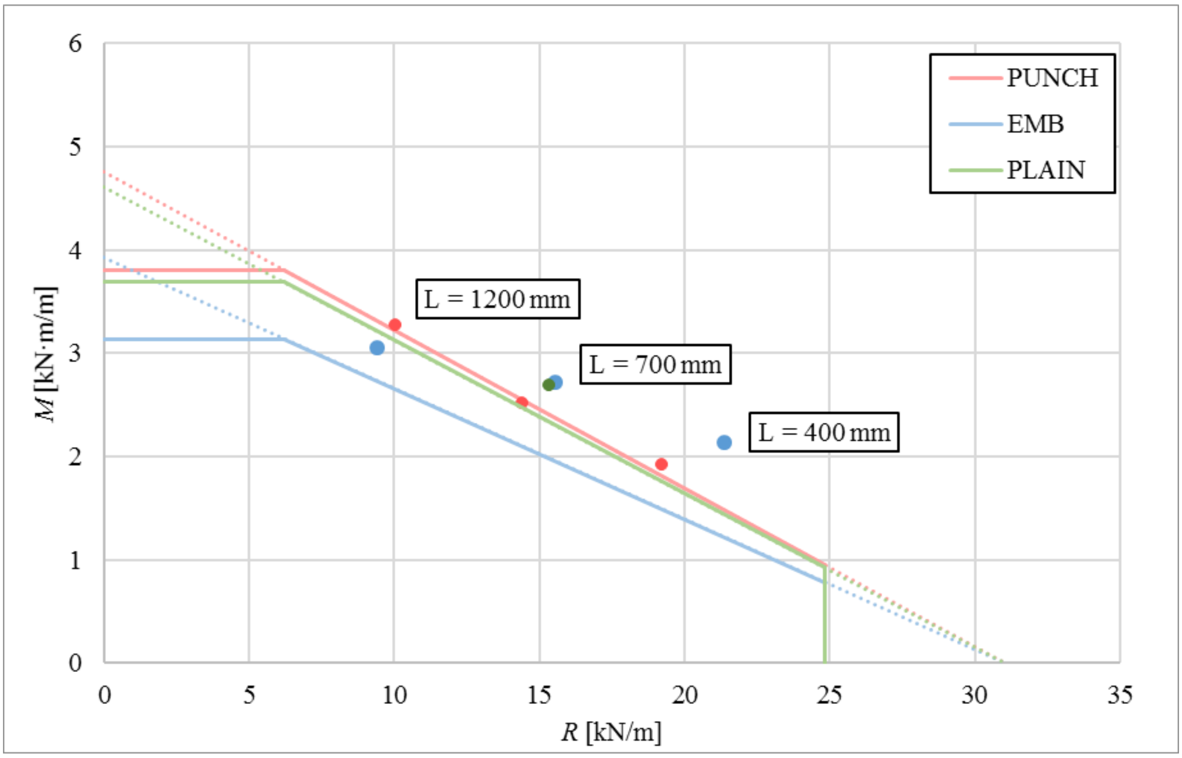

Fig. 18. $M^{-}_{c,Rd} - R_{W,Rd}$ **interaction diagram. t = 0.75 mm.**

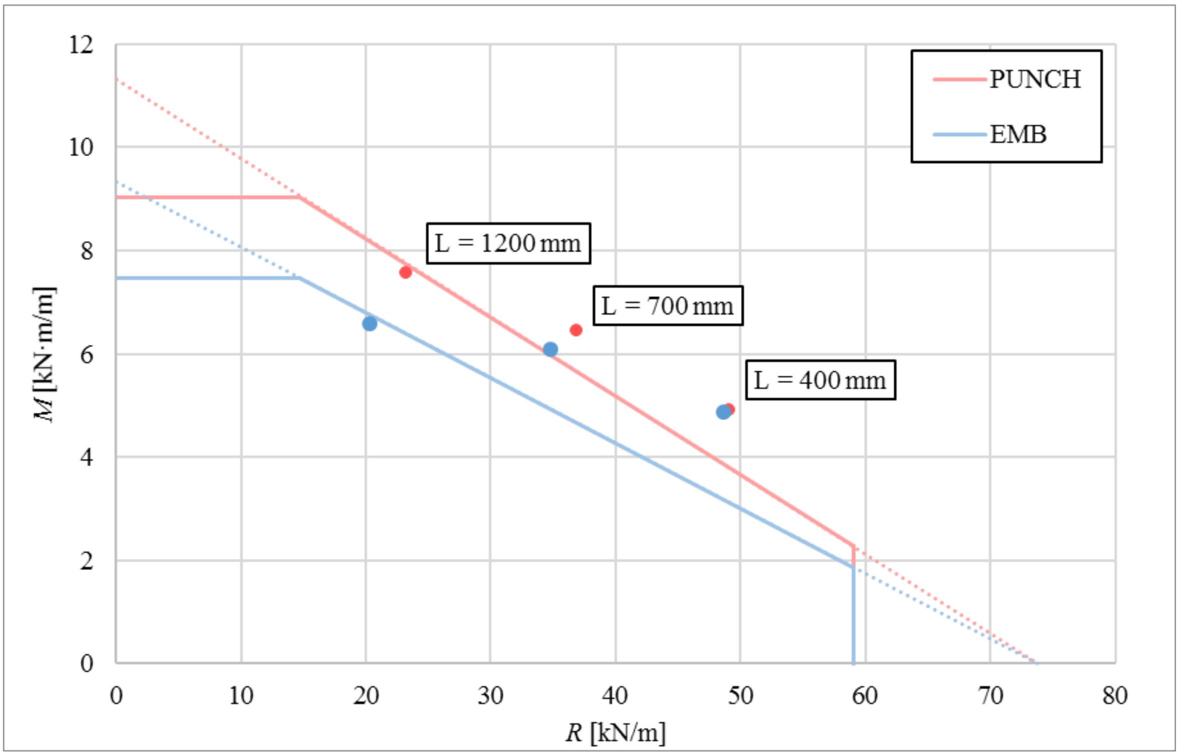

Fig. 19. $M^{-}_{c,Rd} - R_{W,Rd}$ **interaction diagram. t = 1.20 mm.**

7. Analytical method

An analytical study has been carried out to delve deeper into the behaviour of the sheeting and to verify the experimental results.

Inertia and section modulus have been found through different analytical methods. It is important to differentiate three types of results: plastic properties, elastic effective properties and elastic gross properties. All these properties has been calculated following the precepts given in Eurocode. The different methods are almost the same for the three designs, the difference was only the way that the webs were treated.

The elastic gross properties of the cross-section have been calculated to show the behaviour of the sheeting if considered as all effective, without any buckling phenomenon.

For the W60-MD design, a reduced thickness was used in the web (Fig. 20) in order to take into account the reduction of material due to the perforations. This thickness was extracted from EN 1993-1-3:2006 [1], Section 10.4., shown in eq. (13); and GRISPE PLUS D3.1: PERFORATED PROFILES [5], eq. (14).

Fig. 20. Scheme of W60-MD cross-section, with a reduced thickness in the web.

$$t_{a,eff} = 1.09 \cdot t \cdot \left(1 - \frac{1.03 \cdot d}{a}\right) \tag{13}$$

$$t_{a,eff} = 1.18 \cdot t \cdot \left(1 - \frac{0.9 \cdot d}{a}\right) \tag{14}$$

The difference between this two models is the position of the perforations in the web. The formula from the

Eurocode assumes that the punches distribution is staggered (Fig. 21 left) while the GRISPE formula considers an orthogonal distribution (Fig. 21 right).

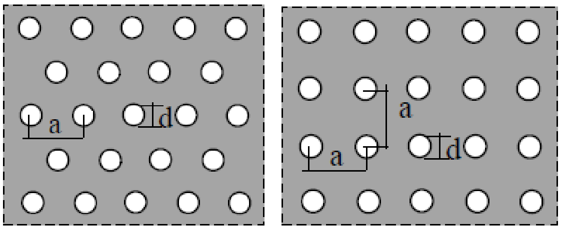

Fig. 21. Distribution and dimension of the perforations according to EN 1993-1-3 [1] (left) and GRISPE PLUS [5] (right).

These two methods need some requirements to be accomplished. First, this models are valid for net holes, i.e., perfect circles in the webs from where the material from the perforation is extracted. The second is a geometrical condition: $0.2 \leq d/a \leq 0.9$.

It must be noted that none of the assumed distributions by the analytical formulas coincide with the actual designs. In addition, the condition of holes is not fulfilled either, although the real material remaining in the crown of the perforations is minimum. However, the geometrical condition is met. Therefore, the two formulas will be used to make a fairly approximation of the sheeting behaviour.

No reduced thickness has been used for the W60-Plain design, since its web is complete and plain.

In the W60-Emb design, the geometry of the embossed web has been taken into account by taking the cross-section right at the symmetry plane of the embossment (Fig. 22).

Fig. 22. Scheme of W60-Emb cross-section, taken at the embossment symmetry plane.

The plastic properties of the section have been calculated to represent the whole yielding of the cross-section.

In the W60-MD design, the cross-section is taken with two perforations only (Fig. 23), since the punches distribution is staggered.

Fig. 23. Scheme of W60-MD design cross-section, taking 2 perforations into account.

The W60-Emb and W60-Plain designs use the same geometry explained in the case of elastic gross properties.

Finally, the elastic effective properties have been calculated. These are the ones that should lead to the most realistic calculations since an elastic behaviour and the possibility of buckling is included.

In the W60-MD design, a reduced thickness has been used to take into account the perforations. The formula was also extracted from section EN 1993-1-3:2006, section 10.4 [1] and GRISPE PLUS D3.1: PERFORATED PROFILES [5], eq. (15) is the same from both references. The profile must meet the same requirements as for the elastic gross properties.

$$t_{b,eff} = t \cdot \sqrt[3]{1.18 \cdot \left(1 - \frac{d}{a}\right)} \tag{15}$$

No reduced thickness has been used for the W60-Plain design, since its web is complete and plain.

In the W60-Emb design, the GRISPE PLUS D3.1: STEEL DECKS WITH EMBOSSENTS [6] recommendation has been used. This document states some conditions for using the method: the first one states that only the resistance of sheeting to bending moment, to local load or support reaction and to a combination of the previous ones can be calculated; the second one is geometric (Fig. 24).

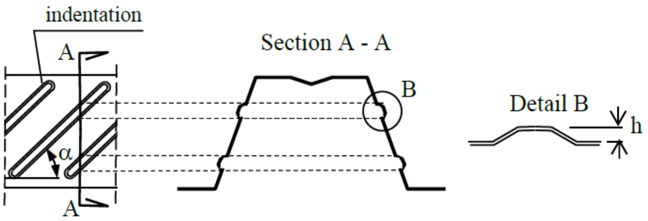

$0.71 \le t \le 1.21$ mm

$h \le 0.9$ mm

$30° \le \alpha \le 60°$

Fig. 24. Embossed profiles according to GRISPE PLUS [6].

The first condition is accomplished, since the bending strength is calculated. Contrary, the second requirement is not met because the embossments angle is 90°, out of the valid range. However, this method has also been presented because a good approximation of the behaviour has been extracted.

It must be noted that the calculations used for the positive and the negative bending moment are slightly different because of the partial plasticity observed in the case of positive bending test, whose *F-d* curve does not have a fairly constant slope as in the case of negative bending moment (Fig. 25). This is because of a small yielding in the tensile flange of the section (Fig. 26) and, therefore, a plastic failure is developed.

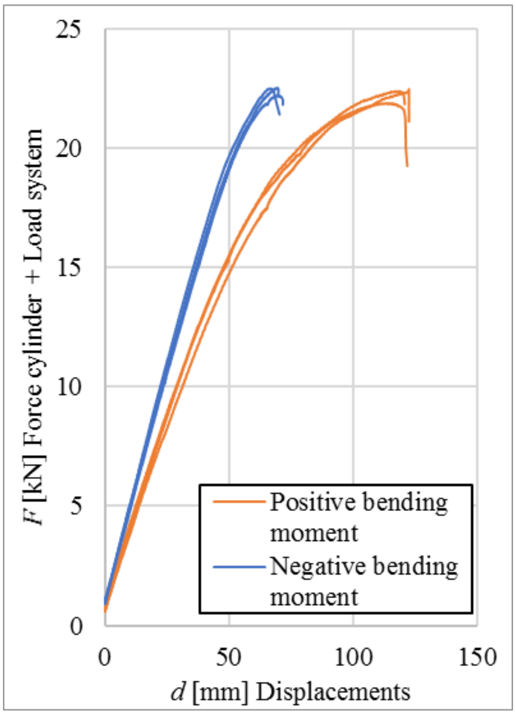

Fig. 25. Comparative between positive and negative F-d curves.

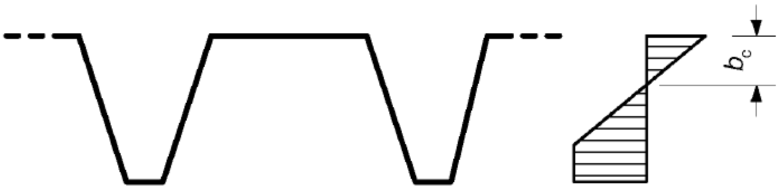

Fig. 26. Stress distribution in partial yielding [3].

Regarding the W60-MD analytical and experimental comparative graphs shown in Fig. 27 to Fig. 30, and the comparative graphs shown in Fig. 31 and Fig. 32 related to all of the three analysed designs, the following aspects can be stated:

i) **Positive bending**: the experimental results are almost equal to the effective ones found through the analytical method.

- for t = 1.20 mm, the experimental and effective results are practically the same as the plastic results. Therefore, almost the whole cross-section is yielded, having an almost fully plastic behaviour.
- for t = 1.00 mm, the experimental and effective results are closer to the plastic results curve than to the elastic gross results. Therefore, a significant part of the cross-section is yielded, being closer to a plastic behaviour than elastic.
- for t = 0.75 mm, the experimental and effective results are closer to the elastic gross results curve than to the plastic results. Therefore, only a small part of the section is yielded, becoming closer to an elastic behaviour than plastic. In the particular case of the W60-Plain design, this is much more accentuated and the elastic gross results are practically identical to the experimental and elastic effective results; therefore, the whole section is effective.

ii) **Negative bending**: the experimental results are between the plastic and elastic range and are also quite similar to the analytical gross elastic ones. Therefore, almost the entire section is effective.

- for t = 1.20 mm, the experimental results are closer to the plastic results curve than to the elastic gross results, due to strain hardening. This phenomenon has similar effects than partial yielding.

- for *t* = 1.00 mm, the experimental results are closer to the plastic results curve than to the elastic gross results but not as close as of *t* = 1.20 mm case. There is some strain hardening but not as much as the previous one.
- for *t* = 0.75 mm, the experimental and effective results are closer to the elastic gross results curve than to the plastic results. Therefore, there is neither partial yielding nor strain hardening.

An apparent incongruence can be observed in the Fig. 27 since the gross elastic results are lower than the effective elastic. The reason for this is the reduced thickness by Eurocode and GRISPE for the gross elastic calculations is lower than the effective one, where, in addition, the whole section is considered.

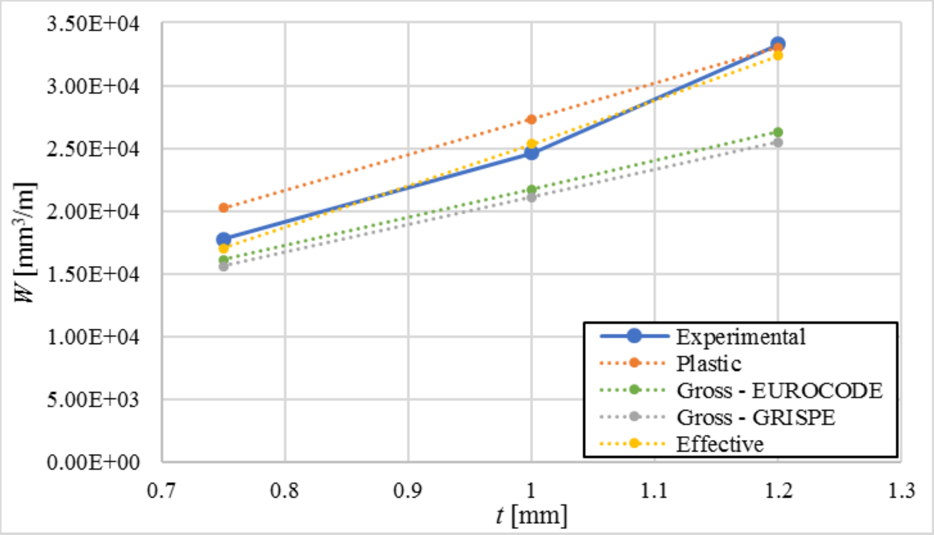

Fig. 27. Section modulus for W60-MD in positive bending.

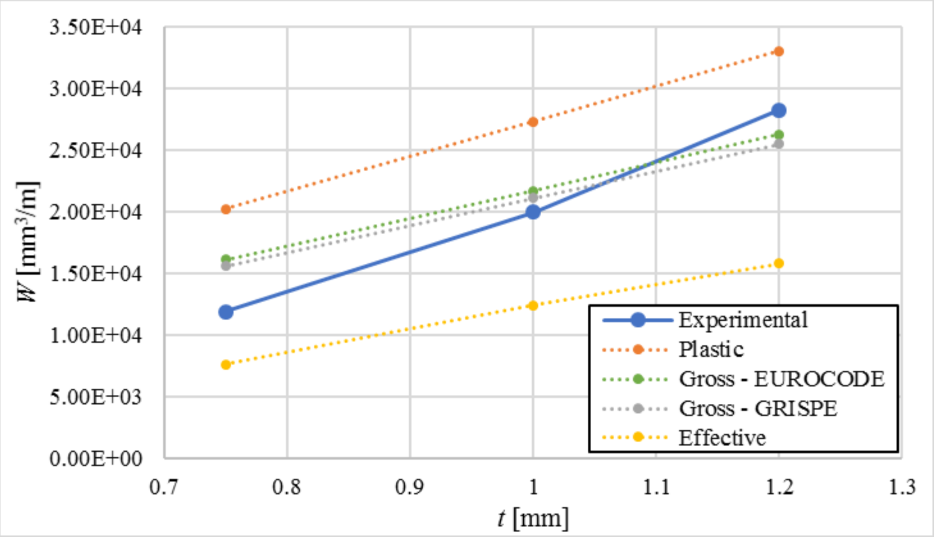

Fig. 28. Section modulus for W60-MD in negative bending.

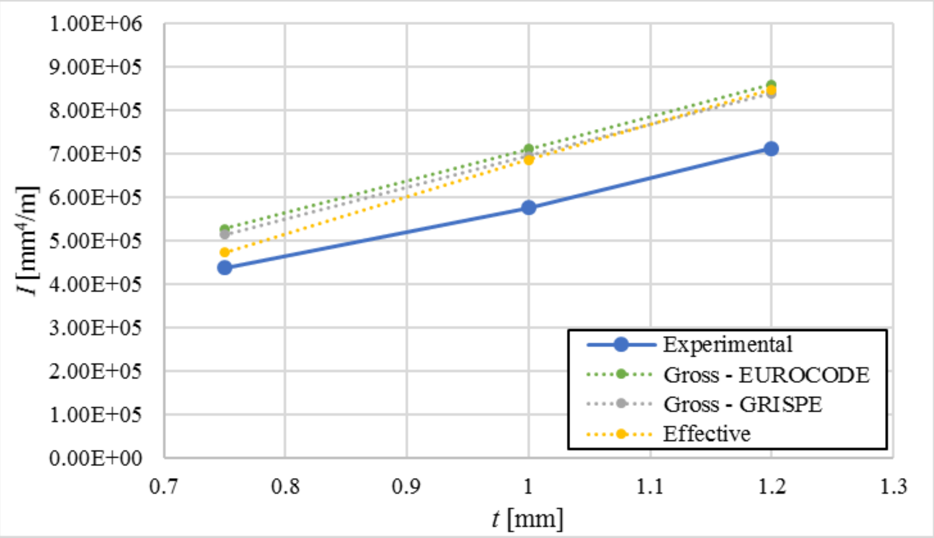

Fig. 29. Inertia for W60-MD in positive bending.

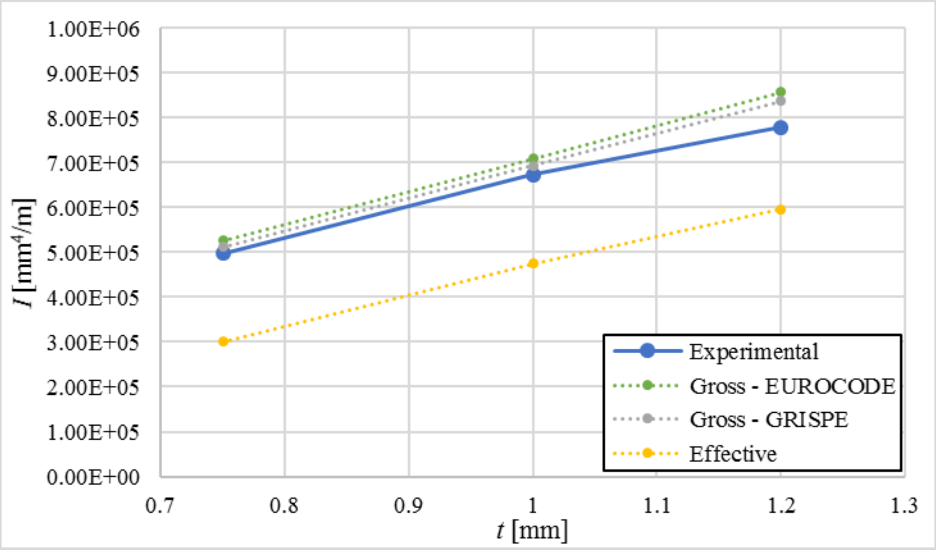

Fig. 30. Inertia for W60-MD in negative bending.

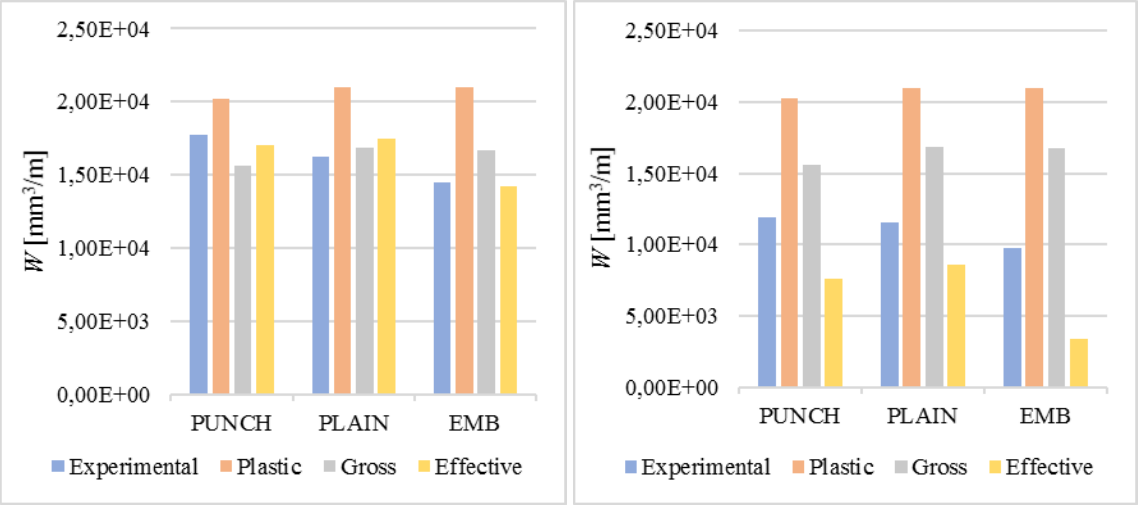

a) *b)*

Fig. 31. Comparison between the section modulus calculations. a) Positive bending b) Negative bending.

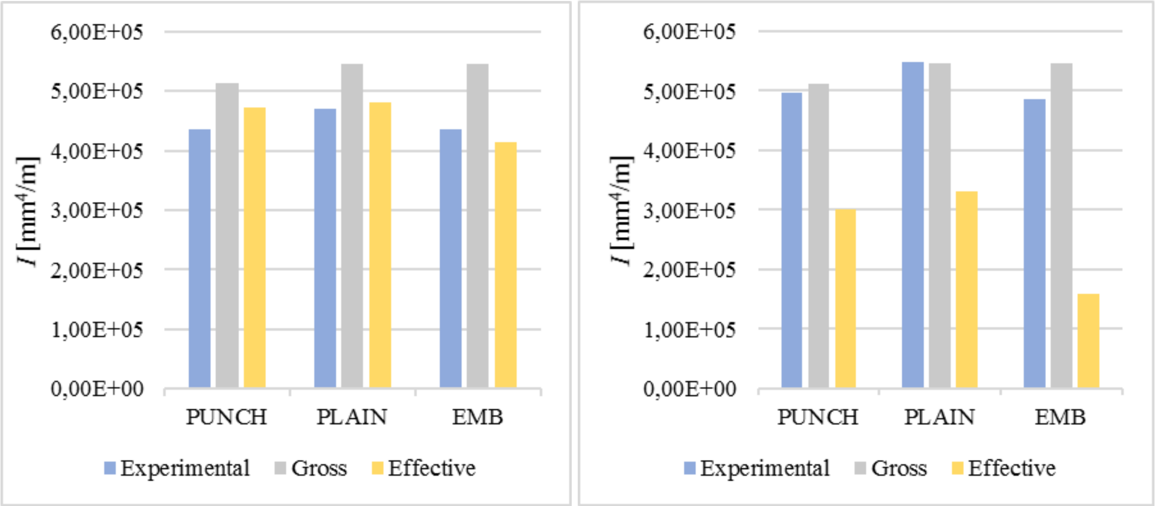

a) *b)*

Fig. 32. Comparison between the moment of inertia calculations. a) Positive bending b) Negative bending.

8 Conclusion

This research shows that the significant improvement in the composite action contributed by the new perfect bond UPC-system **¡Error! No se encuentra el origen de la referencia.** to the steel-concrete composite slabs [2] is not devaluated at all in the construction stage, where the sheeting is resisting the self-weight of the fresh concrete. Contrary, in most cases, the strength of the UPC-system sheeting design is even higher than both the conventional embossed and the plain designs.

Other technical findings can be summarized as follow:

1) A good performance of the UPC-system punched sheeting in the construction stage has been demonstrate and a good agreement of experimental tests has been verified through the moment-reaction interaction diagram with respect to different theoretical calculation methods.

2) Both positive and negative single span bending tests have given the verified values for the moment of inertia and the respective section modulus.

3) The most remarkable conclusion from the internal support tests results is that the W60-MD punched design has shown better performance than W60-Emb for most of the combinations span length – thickness, except in the case of thickness 0.75 mm with short lengths (400 and 700 mm); in this two cases, the load capacity was about 10% lower, which is not really significant.

4) The same properties were found analytically following both Eurocode-3 and GRISPE-PLUS methods. These results have acceptably described the real behaviour.

5) A partial yielding of the cross-section is observed in the case of positive bending, while the behaviour is is completely elastic under negative bending.

Funding

All tests included in this work corresponds to the standard tests required by the Spanish company Europerfil, S.A. in order to characterize the W60-MD sheeting and to verify the benefits of including the UPC-System.

Acknowledgments

The authors want to thank the Master candidate Carla Ripoll and the lab technician Francesc J. Garcia for their kind collaboration.

REFERENCES

[1] Ferrer, M; Marimon, F. Sistema para la conexión entre chapa de acero y hormigón / System for connecting together steel sheet and concrete. Patent ES2344389, EP2305911, WO2010037876. Applicant: Universitat Politècnica de Catalunya.

[2] Ferrer, M., Marimon, F. & Casafont, M. An experimental investigation of a new perfect bond technology for composite slabs.

Construction and Building Materials 166 (2018): 618–633. https://doi.org/10.1016/j.conbuildmat.2018.01.104

[3] CEN (European Committee for Standardization) EN 1993-1-3: Eurocode 3. Design of steel structures. Part 1-3: General rules- Supplementary rules for cold-formed sheeting. Brussels, 2006.

[4] CEN (European Committee for Standardization) EN 1990-1-3: Eurocode 0. Eurocode. Basis of structural design. Brussels, 2002.

[5] Anna Palisson. GRISPE PLUS D3.1: Perforated profiles. France, 2018. http://www.grispeplus.eu/wp-content/uploads/2017/09/Profiles_perforations_V2.pdf. The guidelines and recommendations for integrating specific profiled steel sheets in the Eurocodes (GRISPE) project funded by European Community's Research Fund for Coal and Steel (RFCS).

[6] Anna Palisson. GRISPE PLUS D3.1: Steel decks with Embossments. France, 2018. http://www.grispeplus.eu/wp-content/uploads/2017/09/Steel-decks-Embossments_V5.pdf. The guidelines and recommendations for integrating specific profiled steel sheets in the Eurocodes (GRISPE) project funded by European Community’s Research Fund for Coal and Steel (RFCS).